Shot noise control in coherent nanoscale conductors

Zur Erlangung des akademischen Grades eines
Doktors der Naturwissenschaften
der Mathematisch–Naturwissenschaftlichen Fakultät
der Universität Augsburg vorgelegte

Dissertation

von

Dipl.-Phys. Michael Straß

aus

Donauwörth

Augsburg, im Januar 2006

Erstberichterstatter:	Priv. Doz. Dr. Sigmund Kohler
Zweitberichterstatter:	Prof. Dr. Ulrich Eckern
Tag der mündlichen Prüfung:	15. März 2006

Contents

Important acronyms and symbols

CDT	coherent destruction of tunneling (see chapter 4)
I–V	current–voltage
PAT	photon-assisted tunneling (see chapter 6)
RWA	rotating-wave approximation (see chapter 4)
TLS	two-level system (see chapter 5)
n	index of wire site ($n = 1, \ldots, N$)
ℓ	lead index ($\ell =$ L: left, $\ell =$ R: right)
n_ℓ	wire site connected to lead ℓ ($n_\mathrm{L} = 1$, $n_\mathrm{R} = N$)
α, β	indices of Floquet state
k	sideband/Fourier index
Ω	angular frequency of driving field
$\mathcal{T}$	driving period ($= 2\pi/\Omega$)
Δ	tunneling matrix element of adjacent wire sites
$c_n^\dagger, c_n$	creator and annihilator of wire electron in site n
$c_{q\ell}^\dagger, c_{q\ell}$	creator and annihilator of lead electron
$\lvert n\rangle$	wire site, orbital ($n = 1, \ldots, N$)
$\lvert\chi_\alpha(t)\rangle, \lvert\phi_\alpha(t)\rangle$	Floquet states, Floquet modes
$\epsilon_\alpha - i\hbar\gamma_\alpha$	complex quasienergy

$G(t,t')$	retarded Green function
$G^{(k)}(\epsilon)$	Fourier coefficient of retarded Green function
Σ	imaginary part of self-energy
$\Gamma_\ell(\epsilon)$	spectral density of lead ℓ
$\xi_\ell(\epsilon)$	noise operator of lead ℓ
$f(\epsilon)$	Fermi function ($= [1+\exp(\epsilon/k_\mathrm{B}T)]^{-1}$)

1. Introduction

The development in chip technology over the past 50 years has been truly breathtaking. As a consequence of the ongoing miniaturization, we have reached a situation where the fabrication of integrated circuits based on complementary metal oxide semiconductors (CMOS) encounters severe limitations. The structure size of the next chip generation expected in 2007 will be 45 nm with a gate oxide that is only three atoms thick. Pursuing the top-down approach further by manufacturing with the help of lithography even smaller structures, undesirable quantum mechanical effects like tunneling start to play a decisive role. The tunneling of electrons results in considerable leakage currents which is one of the main issues in microelectronics nowadays (Narendra and Chandrakasan, 2005).

A conceptually different idea is the bottom-up method approaching from the other side: Atoms or molecules constitute the functional units of integrated circuits at the nanoscale. This idea initiated the field of molecular electronics. A milestone of molecular electronics is the paper by Aviram and Ratner (1974) in which they suggested electrical rectification by a single molecule with suitable asymmetry. One of the first experiments in the field has been performed by Mann and Kuhn (1971) who studied the transport through alkane chains in ordered Langmuir-Blodgett monolayers. The Langmuir-Blodgett technique and self-assembly are by now a standard way to form a monolayer of molecules on a surface (Ulman, 1991). By sandwiching such a film between metal electrodes, a rectification effect characterized by an asymmetric current–voltage curve has been observed (Geddes et al., 1992; Metzger et al., 1997). Meanwhile, there exists a rich variety of molecular rectifiers (for an exhaustive survey see Metzger, 2003).

All the measurements discussed so far have in common that presumably many molecules are involved in the electron transfer. A very elegant way for probing conductance through single molecules is the technique of mechan-

ically controllable break-junctions which has been developed in the context of atomic point-contact experiments (for a recent review see Agraït et al., 2003). The first experiment of this kind by Reed et al. (1997) used molecules bonding via thiol groups to the gold electrodes of an open break-junction. They concluded from conductance measurements that the number of active molecules could be as few as one. A similar but more systematic and clear-cut experiment has been performed by Reichert et al. (2002, 2003) using both a symmetric and an asymmetric molecule. The symmetry properties of the sample are reflected in the current–voltage characteristics. This as well as the sample to sample fluctuations in the conductance clearly pointed at transport mediated by an individual molecule. A large number of review articles, special issues and books on the topic of molecular electronics have been published recently (Joachim et al., 2000; Hänggi et al., 2002; Heath and Ratner, 2003; Nitzan and Ratner, 2003; Cuniberti et al., 2005).

The investigation of transport phenomena in such nanoscale conductors is a fascinating field. In order to gain a more profound insight into the physics at work, the examination of the noise characteristics in small electric conductors proves to be a powerful tool (Blanter and Büttiker, 2000; Beenakker and Schönenberger, 2003; Kohler et al., 2005). This is best summarized by the saying of Rolf Landauer: "The noise is the signal." From an experimental point of view, an instructive noise signal in nanoconductors is extremely small and it is a challenging task to detect fluctuations which can be solely attributed to features of the conductor itself. The mostly undesired background noise inherent to the measuring apparatus might be of the same order of magnitude and might even exhibit similar characteristics. Noise in electrical currents was first discussed by Schottky (1918) for vacuum tubes, where the current in the device fluctuates due to the stochastic nature of the electron emission process. This so-called shot noise possesses a spectral density which is proportional to the time-averaged current. However, if quantum coherence is important for the electrical conduction, then noise properties different from shot noise are to be expected. Exploring theoretically the noise behavior of conductors helps to interpret experimental results and might yield suggestions for improving the setup.

In order to construct useful devices, however, it is not sufficient to have a

current flowing through a molecule, but one also needs the ability to control this current. This can in principle be achieved by the so-called single electron transistor setup in which a gate electrode is placed close to the molecule. Applying a gate voltage thus allows influence upon the transport across the molecule. In more complex circuits, the need for a large number of contacts or electrodes close to the molecule may constitute a major obstacle. In fact, already the implementation of a single gate electrode which creates a sufficiently strong field at the molecule is a demanding task (Liang et al., 2002; Zhitenev et al., 2002; Lee et al., 2003). Therefore, other means of controlling the current through a nanosystem should be explored.

One possibility is to replace the static field of a gate electrode by a suitable external ac field. Recent theoretical work by Lehmann et al. (2003a) has demonstrated that, by using a coherent monochromatic field, one should indeed be able to control the electrical current flowing through a nanosystem connected to several leads. In the present work, we extend this idea and investigate the influence of an alternating field in a two-terminal device on the noise characteristics. The molecule connects the two metallic electrodes in the manner of the open break-junction experiments. A possible realization of those periodically driven systems are molecular wires exposed to infrared laser excitation. The corresponding experiments are still in their infancy. Many problems arise resulting from thermal effects both in the electrodes and the tunneling contact (Weber and Würfel, priv. communication).

A more promising approach to conduction experiments in driven nanoconductors is the implementation of quantum dots. They are often referred to as artificial atoms (Kastner, 1993; Blick et al., 1996) since the confinement of the electrons in space leads to the formation of a discrete energy spectrum resembling that of atoms. Quantum dots can be manipulated in a very controlled way so as to pronounce physical effects of interest. For instance the coupling to the electrodes can be tailored via the thickness of the tunneling barriers. Also the level structure within a dot can be readily tuned by means of appropriate gate voltages.

Very intriguing effects like nonadiabatic electron pumping (Wagner and Sols, 1999; Levinson et al., 2000) can be observed in coherently coupled dots. A double lateral quantum dot coupled in series and capacitively driven

by microwaves might be operated as a quantum pump (Oosterkamp et al., 1998): If no external bias voltage is applied, this ac driven setup yields an dc current provided that a spatial asymmetry is present. Electron pumps can be regarded as a mesoscopic realization of the ratchet effect: Counterintuitively to the second law of thermodynamics, directed transport occurs although the net bias of all external forces vanishes (Feynman et al., 1963; Jülicher et al., 1997; Reimann, 2002; Astumian and Hänggi, 2002). This thesis goes beyond existing theoretical studies (Stafford and Wingreen, 1996; Brune et al., 1997) and explores the shot noise behavior of coupled quantum dots for nonadiabatic driving.

Based on the idea of Landauer (1957), coherent transport of electrons can be interpreted as scattering processes across the conducting region. As a result, the conductance is expressed in terms of transmission probabilities. The physical understanding of static transport through mesoscopic structures in terms of quantum mechanical scattering events is well established (Landauer, 1992; Datta, 1995; Imry, 1997; Imry and Landauer, 1999). We derive a generalized scattering formalism extending the Landauer approach to periodic time-dependent systems. In particular, our expressions for the time-averaged current and the current fluctuations are valid for arbitrary driving frequency and strength and for arbitrary coupling strength of the nanoscale conductor to the leads. Formal expressions for the current have been derived for instance by Datta and Anantram (1992) and Jauho et al. (1994) employing nonequilibrium Keldysh techniques. Unlike these authors, we will make use of the time-periodicity of the system.

Outline of the present work

This thesis is organized as follows. In chapter 2, the model system is introduced, where the conductor is described in a tight-binding approximation as a linear chain of orbitals and the terminating sites couple to the metallic leads. The current and the associated noise are computed in terms of the single-particle Green function, therefore effectively our method is restricted to noninteracting electrons. An efficient method for constructing the retarded Green function is presented in terms of a Floquet-Green formalism in chapter 3. In addition, the effect of certain symmetries on the Floquet

states is discussed there. We address in chapter 4 the analytical solution of the time-dependent system at hand in the spirit of a rotating-wave approximation. A particular challenge represents the consistent treatment of the connecting leads in presence of ac fields. Chapter 5 is dedicated to the shot noise control in a driven two-level system. This is closely related to the phenomenon of coherent destruction of tunneling which was discussed the first time for an isolated system by Grossmann et al. (1991) and is briefly recapitulated in the chapter 4. In chapter 6, a realization of a nonadiabatic electron pump in terms of two coherently coupled quantum dots is presented. In particular, we study the noise characteristics of the setup aiming for an optimization of the system parameters. Appendix A comprises the electronic transport quantities of particular static tight-binding systems.

2. Time-dependent scattering formalism

The quantum transport in nanoscale conductors exposed to time-dependent external fields is of course mainly manifested by the dc current through the system. Yet, to learn more about the actual nature of transport, the noise characteristics is even more revealing. In order to account for the symmetry of the many-particle states of electrons, the transport problem is formulated in second quantization. Thereby one ensures a consistent and elegant description to avoid conceptual errors, as for instance not including the Pauli exclusion principle properly. We will derive explicit expressions for the current and the associated noise power in terms of the retarded Green function by solving the Heisenberg equations of motions for the electron creation and annihilation operators. The retarded Green function solves the corresponding Schrödinger equation and therefore fully describes the coherent electron transfer through the nanoconductor. A very important step is the elimination of the electronic states of the leads. In the reduced system, we account for the influence of the metallic leads by a self-energy term. The derivation presented here follows basically the line of reasoning of Kohler et al. (2005) and Hänggi, Kohler, Lehmann, and Strass (2005).

The intuitive physical picture behind the presented formalism allows one interpret the transport in terms of inelastic scattering events incorporating transmission probabilities (Camalet et al., 2003, 2004). At the end, we arrive at an expression for the current which assumes a Landauer-type form, however, generalized for time-dependent systems and valid beyond the linear response regime, *i.e.*, for arbitrary driving strength and coupling to the metallic leads.

In this chapter we make use of the time-periodicity of the driven conductor already to a certain extent. Nonetheless, a practicable form of the retarded Green function in terms of Floquet states and quasienergies will not be presented until the next chapter.

2.1. The model system

To set the stage, the basic working model is introduced. The central conducting region referred to as the wire in the following is sandwiched between two lead contacts. The related time-dependent Hamiltonian can be written in compact form as

$$H(t) = H_{\text{wire}}(t) + H_{\text{leads}} + H_{\text{contacts}} \ , \tag{2.1}$$

in which the individual terms describe the driven quantum wire, the electron reservoirs in the leads, and the coupling of the leads to the wire. To model for instance the macroscopic contacts of a realistic metal–molecule–metal junction is a challenging task already (*e.g.*, Yaliraki and Ratner, 1998; Xue and Ratner, 2003b). Here we focus on phenomena which originate solely from the driving of the wire itself. Furthermore, no influence of the external field on the leads is assumed and consequently the time-dependence only enters via the wire part. For molecular wires which are subject to infrared laser light, this is a rather crude approximation. At least thermal effects are to be expected (Weber and Würfel, priv. communication). However, we can certainly exclude driving-induced photo-electrons stemming from the leads, since the frequency of a laser in the infrared is below the work function of common metals. Note that these approximations, related with the leads, are not an issue for the coupled quantum dots driven by a central ac gate voltage, as the driving field does not affect the lead contacts.

A further simplification is the disregard of electron–electron interaction, which is well justified for few electron systems. Also, electron spin is neglected for simplicity assuming for instance the injection of spin polarized electrons onto the wire. In addition, the wire couples to no other environmental degrees of freedom than the leads.

Within the framework of a tight-binding approximation, the time-dependent wire Hamiltonian consisting of N localized states, each representing a site, reads

$$H_{\text{wire}}(t) = \sum_{n,n'}^{N} H_{nn'}(t) c_n^\dagger c_{n'} \ . \tag{2.2}$$

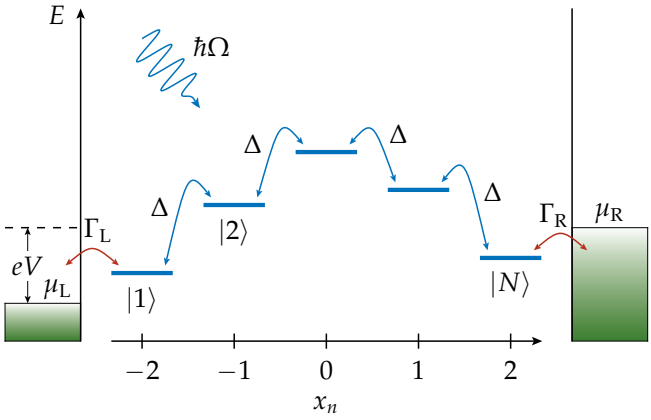

Figure 2.1: Driven tight-binding system consisting of $N = 5$ sites where the uniform intersite coupling is characterized by the tunneling matrix element Δ. The wire is attached to the leads described via the coupling constants Γ_L and Γ_R. A time-periodic external force acts solely on the wire quantified by the driving with the angular frequency Ω and the field strength along the axis of extension. Each site position is scaled by a factor x_n. In addition, a voltage drop $V = (\mu_\mathrm{R} - \mu_\mathrm{L})/e$ is applied.

Depending on the investigated physical system, the matrix elements $H_{nn'}(t)$ will be specified in the appropriate sections. Also the localized states reflect either molecular orbitals (Hückel model) or discrete states in quantum dots which can be interpreted as artificial orbitals. The energy diagram of the paradigmatic model is sketched in Fig. 2.1. The fermion operators c_n, $c_n^\dagger$ destroy and create, respectively, an electron in the state $|n\rangle$. As usual, these operators obey the anticommutation relations $[c_n, c_m^\dagger]_+ = \delta_{nm}$ and $[c_n, c_m]_+ = [c_n^\dagger, c_m^\dagger]_+ = 0$ implying that the states are mutually orthonormal. Of particular interest is the time-periodicity of the wire Hamiltonian $H_{nn'}(t) = H_{nn'}(t + \mathcal{T})$ due to the external alternating field with the angular frequency $\Omega = 2\pi/\mathcal{T}$ of the driving. It eventually allows applying Floquet theory for an efficient treatment of the time-dependent problem.

The metallic leads are described as ideal Fermi gases, *i.e.*, noninteracting

electrons by means of the Hamiltonian

$$H_{\text{leads}} = \sum_{q} \sum_{\ell=\text{L,R}} \epsilon_q c^\dagger_{q\ell} c_{q\ell} \ , \tag{2.3}$$

where the operator $c^\dagger_{q\ell}$ and $c_{q\ell}$ creates and annihilates respectively, an electron in the lead ℓ with energy ϵ_q. Since the lead states are orthogonal to the wire states, the anticommutation rules $[c_n, c^\dagger_{q\ell}]_+ = [c_{q\ell}, c^\dagger_n]_+ = 0$ hold. Naturally, for the wire states the relations $[c_{q\ell}, c^\dagger_{q'\ell'}]_+ = \delta_{\ell\ell'}\delta_{qq'}$ and $[c_{q\ell}, c_{q'\ell'}]_+ = [c^\dagger_{q\ell}, c^\dagger_{q'\ell'}]_+ = 0$ are fulfilled. To fully specify the dynamics of the system, we employ as initial conditions for the electrons in the leads a grand-canonical ensemble at temperature T and with the electro-chemical potentials $\mu_{\text{L,R}}$. The uncorrelated lead electrons are described by the equilibrium Fermi function $f_\ell(\epsilon_q) = \{1 + \exp[(\epsilon_q - \mu_\ell)/k_\text{B}T]\}^{-1}$ which implies at initial time t_0 the density matrix

$$\rho_0 \propto e^{-(H_{\text{leads}} - \mu_\text{L} N_\text{L} - \mu_\text{R} N_\text{R})/k_\text{B}T} \ . \tag{2.4}$$

The operator $N_\ell = \sum_q c^\dagger_{q\ell} c_{q\ell}$ counts the electrons in the respective lead. Eventually, all expectation values of the lead operators can be traced back to the expression

$$\langle c^\dagger_{q'\ell'} c_{q\ell} \rangle = \delta_{\ell\ell'}\delta_{qq'} f_\ell(\epsilon_q) \ . \tag{2.5}$$

Furthermore, an external bias voltage V is mapped to the difference in chemical potentials of the lead contacts as indicated in Fig. 2.1: $V = (\mu_\text{R} - \mu_\text{L})/e$, where $-e$ is the electron charge. Note that the case of oscillating bias voltages in heterostructures is described by our model system (2.1), as well. Camalet et al. (2004) demonstrated that the resulting time-dependence in the lead Hamiltonian can be eliminated by a gauge transformation and transformed to the wire part (2.2).

The terminating orbitals $|1\rangle$ and $|N\rangle$ couple by means of tunneling matrix elements $V_{q\ell}$ to the state $|q\ell\rangle$ in the respective lead. The Hamiltonian which mimics this interaction has the form

$$H_{\text{contacts}} = \sum_q \left(V_{qL} c^\dagger_{qL} c_1 + V_{qR} c^\dagger_{qR} c_N \right) + \text{H.c.} \tag{2.6}$$

As mentioned earlier, we do not aim at modeling the rich structure of the tunneling contacts for molecular junctions. For example Yaliraki et al. (1999) and Xue and Ratner (2003a) argued that the interface has a rather small impact on the conduction. We therefore use a rate description similar to Fermi's golden rule which is well established from tunneling in mesoscopic systems and we do not care for detailed structure of the contact. The tunneling from the lead states which are assumed to be dense to the discrete spectrum in the wire is fully described by the spectral density

$$\Gamma_\ell(\epsilon) = 2\pi \sum_q |V_{q\ell}|^2 \delta(\epsilon - \epsilon_q) \ . \tag{2.7}$$

To derive the expression for the current and its noise in the following, the energy dependence is carried along to preserve the general validity of the presented result. However, to obtain an applicable form for the retarded Green function in terms of the Floquet states in chapter 3, the coupling strength is presumed to be energy independent there:

$$\Gamma_\ell(\epsilon) = \Gamma_\ell = \text{const.} \tag{2.8}$$

This so-called wide-band limit is well justified as long as the bandwidth of the conduction band in the leads is much larger than the energy regime where transport proceeds.

2.2. Electrical current

2.2.1. Landauer scattering approach

Following the idea of Landauer (1957, 1970), the coherent transport for non-interacting electrons can be interpreted as a quantum mechanical scattering process. Thereby the in- and outgoing electronic states scattered in the mesoscopic, possibly disordered conductor are considered as plane waves. The pivotal quantity which determines the conductance of the system is the total transmission probability, which sums over all elastic transmission channels: $T(E) = \sum_n T_n(E)$. Historically, the Landauer formula for the linear conductance was derived for time-independent conductors in the linear

response limit and reads for a two-terminal device

$$G = \frac{e^2}{h} T(E_\mathrm{F}) \ , \tag{2.9}$$

where E_F denotes the Fermi energy. The corresponding static current can be written as

$$I = \frac{e}{h} \int dE \, T(E) \left[f_\mathrm{R}(E) - f_\mathrm{L}(E) \right] \ . \tag{2.10}$$

There exist some generalizations and extensions of this current formula. Just to state a few, derivations of Landauer-type expressions have been presented for the linear conductance of time-independent systems (Fisher and Lee, 1981), for tunnelling barriers (Caroli et al., 1971) and mesoscopic conductors (Meir and Wingreen, 1992) in the static case for finite voltage, and for a wire consisting of levels that couple equally strong to both leads (Jauho et al., 1994).

It has to be emphasized that the scattering approach has contributed a great deal to the understanding of the transport in mesoscopic systems (for a review see Stone and Szafer, 1988). Nonetheless, the Landauer theory was originally postulated *ad hoc*. In the following we will derive rigorously a scattering formalism for the time-dependent system introduced in the previous section.

2.2.2. Heisenberg equations of motion

In order to derive the time-averaged current, we first have to provide an expression for the time-dependent current operator. As a consequence of the continuity equation, the net current traversing the contact ℓ has to be equal to the time derivative of the charge accumulated in that contact with respect to the initial time t_0 since the total charge must be conserved. With the charge operator $Q_\ell(t) = eN_\ell(t) - eN_\ell(t_0)$, the current operator in the Heisenberg picture follows as

$$I_\ell(t) = e \frac{d}{dt} \langle N_\ell \rangle = \frac{ie}{\hbar} \langle [H(t), N_\ell] \rangle \ , \tag{2.11}$$

where $N_\ell = \sum_q c^\dagger_{q\ell} c_{q\ell}$. Hence, we work from now in the Heisenberg picture and have to solve the Heisenberg equations of motion for the annihilation operators in lead ℓ which reads

$$\dot{c}_{q\ell} = -\frac{i}{\hbar}\left(\epsilon_q c_{q\ell} + V_{q\ell} c_{n_\ell}\right) \ , \tag{2.12}$$

where c_{n_ℓ} denotes the terminating sites connected with lead ℓ, *i.e.*, $n_{\mathrm{L}} = 1$ and $n_{\mathrm{R}} = N$. Integrating yields the solution

$$c_{q\ell}(t) = c_{q\ell}(t_0) e^{-i\epsilon_q (t-t_0)/\hbar} - \frac{i}{\hbar} V_{q\ell} \int_{t_0}^{t} dt' \, e^{-i\epsilon_q (t-t')/\hbar} c_{n_\ell}(t') \ , \tag{2.13}$$

where the first term describes the transient behavior. Likewise, the Heisenberg equations of motion for the annihilation operators of wire operators are given by

$$\dot{c}_{n_\ell} = -\frac{i}{\hbar} \sum_{n'} H_{n_\ell n'}(t) c_{n'} - \frac{i}{\hbar} \sum_q V^*_{q\ell} c_{q\ell} \ , \tag{2.14}$$

$$\dot{c}_n = -\frac{i}{\hbar} \sum_{n'} H_{nn'}(t) c_{n'} \ , \quad n = 2, \ldots, N-1 \ . \tag{2.15}$$

Inserting (2.13) into these equations of motion we obtain

$$\dot{c}_{n_\ell}(t) = -\frac{i}{\hbar} \sum_{n'} H_{n_\ell n'}(t) c_{n'}(t) - \frac{i}{\hbar} \int_0^\infty d\tau \, \Gamma_\ell(\tau) c_{n_\ell}(t-\tau) + \xi_\ell(t) \ , \tag{2.16}$$

$$\dot{c}_n(t) = -\frac{i}{\hbar} \sum_{n'} H_{nn'}(t) c_{n'}(t) \ , \quad n = 2, \ldots, N-1 \ . \tag{2.17}$$

Note that here we applied the asymptotic limit $t_0 \to -\infty$ as will be done henceforth. We are not interested in effects that stem from the initial preparation and therefore all transients are eliminated in the long time limit. The previous set of linear coupled equations corresponds to the Quantum-Langevin equations of the system. Having a closer look, the expression containing the lead response function $\Gamma_\ell(t)$ can be interpreted as a damping term. $\Gamma_\ell(t)$ is defined by the Fourier transformation of the spectral density (2.7),

$$\Gamma_\ell(t) = \int \frac{d\epsilon}{2\pi\hbar} e^{-i\epsilon t/\hbar} \Gamma_\ell(\epsilon) \ . \tag{2.18}$$

Making use of the wide-band limit (2.8), the response function becomes $\Gamma_\ell(t) = \Gamma_\ell \delta(t)$. The integro-differential equations of motion then reduce to ordinary differential equations.

In contrast, the operator-valued noise

$$\xi_\ell(t) = \frac{i}{\hbar} \sum_q V_{q\ell}^* \, e^{-i\epsilon_q (t-t_0)/\hbar} c_{q\ell}(t_0) \tag{2.19}$$

reflects a fluctuating force field due to the coupling to the leads which represents a random source of Gaussian distributed electrons. Therefore, from a stochastic point of view, the leads have been eliminated in favor of a stochastic force similar to Grabert et al. (1984) for bosonic environment, but here for fermions. The Langevin equations describe the reduced dynamics of the system. As a consequence of the grand-canonical initial preparation, the noise operator is completely characterized by the relation $\langle \xi_\ell(t) \rangle = 0$ and the correlation function

$$\langle \xi_{\ell'}^\dagger(t-\tau) \xi_\ell(t) \rangle = \delta_{\ell\ell'} \int \frac{d\epsilon}{2\pi\hbar^2} e^{-i\epsilon\tau/\hbar} \Gamma_\ell(\epsilon) f_\ell(\epsilon) \ . \tag{2.20}$$

These expectation values can be derived straightforwardly starting from the definition (2.19) and employing the initial condition (2.4) of uncorrelated lead electrons. The correlation function is very closely related to the lesser Green functions $g_{q\ell}^<(t,t') = i\langle c_{q\ell}^\dagger(t') c_{q\ell}(t) \rangle$ put forward for a similar but time-independent setup by Meir and Wingreen (1992) applying a nonequilibrium Keldysh technique. It fully establishes together with the tunneling matrix elements $V_{q\ell}$ the influence of the leads.

2.2.3. Retarded Green function

The formal solution of the inhomogeneous integro-differential equations (2.16) and (2.17) can be stated in closed form as

$$c_n(t) = i\hbar \sum_{\ell=\mathrm{L,R}} \int_0^\infty d\tau \, G_{nn_\ell}(t, t-\tau) \xi_\ell(t-\tau) \tag{2.21}$$

involving the retarded Green operator $G(t,t') = -(i/\hbar) U(t,t') \Theta(t-t')$. Its matrix elements are defined by $G_{nn'}(t,t') = \langle n | G(t,t') | n' \rangle$. Note that $G(t,t')$

explicitly depends on two times and not just on the time difference in contrast to the static system (see Appendix A). In particular, the equation of motion for the retarded Green function which in fact represents the dynamics of the integro-differential equations assumes the Schrödinger-like form

$$\left(i\hbar\frac{d}{dt} - \mathcal{H}_{\mathrm{wire}}(t)\right) G(t,t') + i\int_0^\infty d\tau\, \Gamma(\tau) G(t-\tau,t') = \delta(t-t') \ . \quad (2.22)$$

Here, $\mathcal{H}_{\mathrm{wire}}(t) = \sum_{n,n'} |n\rangle H_{nn'}(t)\langle n'|$ denotes the single-particle Hamiltonian corresponding to (2.2) and the term $\Gamma(t) = |1\rangle\Gamma_{\mathrm{L}}(t)\langle 1| + |N\rangle\Gamma_{\mathrm{R}}(t)\langle N|$ incorporates the impact of the leads. As a matter of fact, the associated single-particle propagator $U(t,t')$ obeys in the asymptotic limit $t_0 \to -\infty$ the time-periodicity of the wire Hamiltonian caused by the external electromagnetic field (see *e.g.*, Grifoni and Hänggi, 1998), which means

$$U(t,t') = U(t+\mathcal{T},t'+\mathcal{T}) \ . \quad (2.23)$$

This property devolves to the retarded Green function whose Fourier representation reads thus

$$G(t,\epsilon) = -\frac{i}{\hbar}\int_0^\infty d\tau\, e^{i\epsilon\tau/\hbar} U(t,t-\tau) = G(t+\mathcal{T},\epsilon) \ . \quad (2.24)$$

Therefore, we eventually arrived at an expression for the solution of the reduced dynamics of the system. Yet, this only constitutes a formal solution, in the next chapter an applicable form of the retarded Green function will be constructed with the help of Floquet theory.

As a result of the time-periodicity (2.24), the latter expression can also be expanded into the Fourier series $G(t,\epsilon) = \sum_k e^{-ik\Omega t} G^{(k)}(\epsilon)$ with the coefficients

$$G^{(k)}(\epsilon) = \frac{1}{\mathcal{T}}\int_0^{\mathcal{T}} dt\, e^{ik\Omega t} G(t,\epsilon) \ . \quad (2.25)$$

Accordingly, the solution of the wire operator (2.21) can be written in energy representation as

$$c_n(t) = \frac{i}{2\pi}\sum_{\ell=\mathrm{L,R}}\int_{-\infty}^\infty d\epsilon\, e^{-i\epsilon t/\hbar} G_{n,n_\ell}(t,\epsilon)\xi_\ell(\epsilon) \ , \quad (2.26)$$

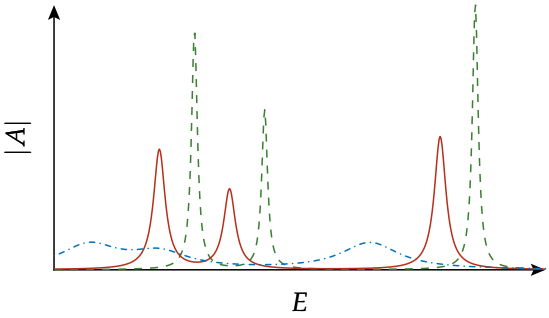

Figure 2.2: Influence of leads on central conducting system. With increasing coupling strength the peaks in the spectral function A are shifted in energy and broadened. For an isolated conductor, the peaks become δ functions

where the Fourier representation of the noise operator is defined as

$$\xi_\ell(\epsilon) = \int dt\, e^{i\epsilon t/\hbar} \xi_\ell(t). \tag{2.27}$$

Physically, the expression under the integral in Eq. (2.22) contains the self-energy term which modifies the energy spectrum (*e.g.*, Datta, 1995, chapter 3). The eigenenergies of the isolated system are renormalized by acquiring an additional, in general complex-valued term. The real part causes a shift in energy and the imaginary part relates to the finite lifetime of an electron injected into the conductor. To exemplify the influence of the leads on the conductor, the spectral function $A = i(G - G^\dagger)$ for different lead–wire coupling strength is depicted qualitatively in Fig. 2.2 illustrating three different coupling situations. Here, $G^\dagger$ denotes the advanced Green function.

Before turning our attention back to the current, we would like to state the very useful identity

$$\begin{aligned} G^\dagger(t,\epsilon') - G(t,\epsilon) = &\left(i\hbar\frac{d}{dt} - \epsilon' + \epsilon\right) G^\dagger(t,\epsilon')G(t,\epsilon) \\ &+ i\int_0^\infty d\tau\, e^{i\epsilon\tau/\hbar} G^\dagger(t,\epsilon')\Gamma(\tau)G(t-\tau,\epsilon) \\ &+ i\int_0^\infty d\tau\, e^{-i\epsilon'\tau/\hbar} G^\dagger(t-\tau,\epsilon')\Gamma^\dagger(\tau)G(t,\epsilon) \end{aligned} \tag{2.28}$$

which corresponds to the identity put forward for the case of weak lead–wire coupling by Datta and Anantram [1992, Eq. (20)]. A proof requires the Fourier transformation of Eq. (2.22) with respect to t' and then multiplying the outcome by $G^\dagger(t,\epsilon)$ from the left. The difference between the resulting expression and its Hermitian adjoint with ϵ and ϵ' interchanged yields the above identity.

2.2.4. Average current

We are now able to proceed onto evaluating the time-dependent current. From the definition (2.11) the expression

$$I_{\mathrm{L}}(t) = \frac{ie}{\hbar}\sum_q \left(V_{q\mathrm{L}}^* c_1^\dagger c_{q\mathrm{L}} - \mathrm{H.c.}\right) \tag{2.29}$$

for the current through the left contact is obtained after a bit of algebra. Upon inserting the Heisenberg operator (2.13) and the definition (2.19) of the noise operator, we arrive at

$$\begin{aligned} I_{\mathrm{L}}(t) = \frac{e}{\hbar}\int_0^\infty d\tau \left[\Gamma_{\mathrm{L}}(\tau)c_1^\dagger(t)c_1(t-\tau) + \Gamma_{\mathrm{L}}^*(\tau)c_1^\dagger(t-\tau)c_1(t)\right] \\ - e\left[c_1^\dagger(t)\xi_{\mathrm{L}}(t) + \xi_{\mathrm{L}}^\dagger(t)c_1(t)\right] \end{aligned} \tag{2.30}$$

and a corresponding expression for $I_{\mathrm{R}}(t)$. Putting this current operator into context with the Keldysh formalism, the terms in the first line can be attributed to the lesser Green functions, whereas the second line stems from contributions of the retarded Green function. As a next step, the mean value of the current is finally determined by the expectation value of the current operator (2.30). By using the solution (2.26) for the wire operator and the correlation function

$$\langle \xi_\ell^\dagger(\epsilon)\xi_{\ell'}(\epsilon')\rangle = 2\pi\Gamma_\ell(\epsilon)f_\ell(\epsilon)\delta(\epsilon-\epsilon')\delta_{\ell\ell'} \ , \tag{2.31}$$

which is the Fourier representation of Eq. (2.20), we obtain

$$\begin{aligned}\langle I_{\mathrm{L}}(t)\rangle = \frac{e}{h}\sum_{\ell=\mathrm{L,R}}\int d\epsilon \int_0^\infty d\tau \big[& e^{i\epsilon\tau/\hbar} G^*_{1\ell}(t,\epsilon)\Gamma_{\mathrm{L}}(\tau)\, G_{1\ell}(t-\tau,\epsilon)\Gamma_\ell(\epsilon) f_\ell(\epsilon) \\ & + e^{-i\epsilon\tau/\hbar} G^*_{1\ell}(t-\tau,\epsilon)\Gamma^*_{\mathrm{L}}(\tau)\, G_{1\ell}(t,\epsilon)\Gamma_\ell(\epsilon) f_\ell(\epsilon)\big] \\ & + ie\int d\epsilon\, [G^*_{11}(t,\epsilon) - G_{11}(t,\epsilon)]\,\Gamma_{\mathrm{L}}(\epsilon) f_\ell(\epsilon)\ .\end{aligned} \tag{2.32}$$

It should be noted that this current formula is valid beyond the linear transport regime describing nonadiabatic driving and holds for any lead–wire coupling. Nonetheless, a scattering-like form in the spirit of the Landauer approach requires us to eliminate the back-scattering terms G_{11} present in the unsymmetric expression (2.32) for the current formula. Here, the last line of the current corresponds to the left-hand side of the identity (2.28) when extracting the appropriate matrix elements G_{11} there. Consequently substituting the back-scattering terms, one arrives at the symmetric form

$$\langle I_{\mathrm{L}}(t)\rangle = \frac{e}{h}\int d\epsilon\, [T_{\mathrm{LR}}(t,\epsilon) f_{\mathrm{R}}(\epsilon) - T_{\mathrm{RL}}(t,\epsilon) f_{\mathrm{L}}(\epsilon)] - \frac{d}{dt} q_{\mathrm{L}}(t) \tag{2.33}$$

for the ac current, where the definition

$$T_{\mathrm{LR}}(t,\epsilon) = 2\Re \int_0^\infty d\tau\, e^{i\epsilon\tau/\hbar}\Gamma_{\mathrm{L}}(\tau) G^*_{1N}(t,\epsilon) G_{1N}(t-\tau,\epsilon)\Gamma_{\mathrm{R}}(\epsilon) \tag{2.34}$$

for the transmission coefficient of an electron transferred from the right to the left lead has been used. Accordingly, for the reversed transmission $T_{\mathrm{RL}}(t,\epsilon)$ the replacement $(\mathrm{L},1) \leftrightarrow (\mathrm{R},N)$ has to be made. Comparing this to the static case (2.10), one immediately realizes that the transmission in the driven situation depends explicitly on time. In addition, the extra term

$$q_{\mathrm{L}}(t) = \frac{e}{2\pi}\int d\epsilon\, \Gamma_{\mathrm{L}}(\epsilon) \sum_n |G_{n1}(t,\epsilon)|^2 f_{\mathrm{L}}(\epsilon) \tag{2.35}$$

occurs, which denotes a periodically oscillating charge between the left lead and the wire. Note that any contributions stemming from a displacement current are contained in this expression.

Upon time-averaging over one driving period $\mathcal{T}$, this charging term will cancel and we obtain as one of the main results in this chapter for the dc current the expression

$$\bar{I} = \frac{e}{h} \sum_{k=-\infty}^{\infty} \int d\epsilon \left[T_{\mathrm{LR}}^{(k)}(\epsilon) f_{\mathrm{R}}(\epsilon) - T_{\mathrm{RL}}^{(k)}(\epsilon) f_{\mathrm{L}}(\epsilon) \right] , \tag{2.36}$$

where the transmission probabilities are given by

$$T_{\mathrm{LR}}^{(k)}(\epsilon) = \frac{1}{\mathcal{T}} \int_0^{\mathcal{T}} dt\, e^{ik\Omega t} T_{\mathrm{LR}}(t, \epsilon) = \Gamma_{\mathrm{L}}(\epsilon + k\hbar\Omega) \Gamma_{\mathrm{R}}(\epsilon) \left| G_{1N}^{(k)}(\epsilon) \right|^2 \tag{2.37}$$

and $T_{\mathrm{RL}}^{(k)}(\epsilon)$, again with L interchanged by R and 1 by N. This definition relates the transmission to the propagator in the spirit of Fisher and Lee (1981). Physically, it describes the propagation of a transmitted electron with initial energy ϵ from one lead to the other lead undergoing scattering events with emission ($k < 0$) or absorption ($k > 0$) of $|k|$ photons, or being transmitted elastically ($k = 0$). The index k is also often referred to as sideband index. Note that for the derivation of the dc current, we made use of the Fourier coefficients (2.25) of the retarded Green function here. Furthermore, the index L for the left contact has been dropped in Eq. (2.36) as a consequence of charge conservation which renders the time-averaged current through the right contact equal, except for the sign.

For the time-independent situation, the transmission functions $T_{\mathrm{LR}}^{(k)}(\epsilon)$ and $T_{\mathrm{RL}}^{(k)}(\epsilon)$ are identical and solely the contributions with $k = 0$ are nonzero. Therefore, it is possible to write the current (2.36) in the form (2.10) as a product of a single total transmission $T(\epsilon)$, which is independent of the direction, and the difference $f_{\mathrm{R}}(\epsilon) - f_{\mathrm{L}}(\epsilon)$ of the Fermi functions. For a driven conductor, this is no longer the case.

2.3. Current fluctuations

2.3.1. Noise power

Experimentally relevant since measurable is the zero-frequency component of the current noise indicating the noise power of a conductor. The noise

through the contact ℓ is defined via the symmetric auto-correlation function of the current fluctuation operator $\Delta I_\ell(t) = I_\ell(t) - \langle I_\ell(t)\rangle$ to read

$$S_\ell(t,t') = \frac{1}{2}\langle [\Delta I_\ell(t), \Delta I_\ell(t')]_+ \rangle \ . \tag{2.38}$$

It explicitly depends on both times as a consequence of the external field. Moreover, the noise possesses for asymptotic times ($t_0 \to -\infty$) the same time-periodicity as the propagator (2.23), $S_\ell(t,t') = S_\ell(t+\mathcal{T}, t'+\mathcal{T})$. Finally, the noise power is obtained by time-averaging the zero-frequency component over one driving period

$$\bar{S} = \frac{1}{\mathcal{T}} \int_0^{\mathcal{T}} dt \int_{-\infty}^{\infty} d\tau \, S_\ell(t, t-\tau) \ . \tag{2.39}$$

Note that similar to the absolute value of the average dc current, the noise power of a two-terminal setup does not depend on the contact ℓ anymore due to charge conservation. This is why the index ℓ has been omitted. To evaluate $\bar{S}$ involves some rather tedious algebra using the current operator (2.30), its expectation value (2.32) and the solution (2.26) of the Heisenberg equations of motion. We want to spare the reader from the details and only state the final result

$$\begin{aligned}\bar{S} = \frac{e^2}{h} \sum_k \int d\epsilon \, \Gamma_{\mathrm{R}}(\epsilon_k) \Bigg\{ & \Gamma_{\mathrm{R}}(\epsilon) \Big| \sum_{k'} \Gamma_{\mathrm{L}}(\epsilon_{k'}) G_{1N}^{(k'-k)}(\epsilon_k) \big[G_{1N}^{(k')}(\epsilon)\big]^* \Big|^2 f_{\mathrm{R}}(\epsilon) \bar{f}_{\mathrm{R}}(\epsilon_k) \\ & + \Gamma_{\mathrm{L}}(\epsilon) \Big| \sum_{k'} \Gamma_{\mathrm{L}}(\epsilon_{k'}) G_{1N}^{(k'-k)}(\epsilon_k) \big[G_{11}^{(k')}(\epsilon)\big]^* - i G_{1N}^{(-k)}(\epsilon_k) \Big|^2 f_{\mathrm{L}}(\epsilon) \bar{f}_{\mathrm{R}}(\epsilon_k) \Bigg\} \\ & + \text{same terms with the replacement } (\mathrm{L},1) \leftrightarrow (\mathrm{R},N) \ ,\end{aligned} \tag{2.40}$$

with the shorthand notation $\epsilon_k = \epsilon + k\hbar\Omega$ and $\bar{f}_\ell(\epsilon) = 1 - f_\ell(\epsilon)$. Again, to arrive at a more compact notation, the identity (2.28) has been applied here. Surprisingly enough, the current noise (2.40) depends on the phase of the transmission amplitudes in contrast to the static situation where only the transmission probability enters (see Eq. (A.5) in the Appendix).

2.3.2. Shot noise

A very insightful quantity characterizing the relative noise strength of a conductor is the so-called Fano factor (Fano, 1947)

$$F = \frac{\bar{S}}{e|\bar{I}|} \quad . \tag{2.41}$$

As a reference point for noise the case of uncorrelated tunneling events denoted as the Poisson value of shot noise $\bar{S} = e|\bar{I}|$ for which $F = 1$ is considered. Shot noise was discussed the first time by Schottky (1918) in connection with vacuum tubes. He explained how electrons are emitted from the cathode with a certain stochastic probability depending on whether they can overcome the work function. Consequently, the resulting particle flux fluctuates randomly around the mean value of the current. Shot noise describes therefore the kinematics of transport processes out of equilibrium which result from the discreteness of the charge carriers. Measuring both the average dc current and the shot noise allowed, for example, the experimental confirmation of the fractional Hall effect predicted by Laughlin (1983). It took some time till de Picciotto et al. (1997) verified for the first time the fractional charge $q = -1/3$.

Pure shot noise corresponds to $F = 1$ meaning that the electrons creating a current are totally uncorrelated. Any value lower than unity indicates shot noise suppression (sub-poissonian noise), whereas any value above unity is called super-poissonian behavior. Note that historically the Poisson value is defined by $2e|I|$ resulting from a different definition—in comparison to our derivation—of the Fourier transform in the noise power. Hence, in order to obtain $F = 1$ for a Poisson process, the factor 2 has been omitted in the Fano factor (2.41).

3. Dissipative Floquet theory

Now that we have derived general expressions for the current and the associated noise in terms of the retarded Green function, we are still obligated to actually compute the Green function. Since the wire is subject to an intense monochromatic field, it is state of the art to treat the external electromagnetic field in a semiclassical approach by means of a dipole approximation (Aravind and Hirschfelder, 1984). We will justify the dipole coupling to the wire in more detail from a physical point of view. Based on the time-periodicity of the driven quantum system, a natural basis for an expansion of the retarded Green function into eigenfunctions is provided by the Floquet ansatz. Floquet theory is well established, for instance, in atomic physics (for a review see Manakov et al., 1986) or quantum tunneling driven by intense, periodic fields (for a review see Grifoni and Hänggi, 1998). Note that for the decomposition into Floquet states the dipole coupling of the external field is not a prerequisite. A Floquet approach is generally applicable for any time-periodic system.

In contrast to usual Floquet theory, we address here a non-Hermitian problem because the nanoscale wire couples to environmental degrees of freedom in terms of the leads. The lead states have been already eliminated in the previous chapter in favor of the self-energy. Therefore we will construct now a solution of the retarded Green function for this dissipative system. A nonunitary propagator and complex eigenvalues are the consequence.

3.1. Solution in composite Hilbert space

3.1.1. Tight-binding system driven by a dipole field

The penalty paid to keep the application of Floquet theory feasible is the fact that we effectively consider noninteracting electrons. Coulomb inter-

action effects could be accounted for by constructing many-particle states based on a Floquet ansatz. However, this is beyond the scope of this work and consequently we consider a single-particle problem. The corresponding time-dependent wire Hamiltonian reads in the tight-binding basis of the orbitals

$$\mathcal{H}_{\text{wire}}(t) = -\Delta \sum_{n=1}^{N-1} (|n\rangle\langle n+1| + |n+1\rangle\langle n|) + \sum_n [E_n + x_n f(t)]|n\rangle\langle n| \ . \quad (3.1)$$

This constitutes a linear chain of orbitals with constant nearest neighbor coupling Δ as sketched in Fig. 2.1 on page 9. Note that Δ depends on the distance of adjacent sites since it is related to the hopping rates of electrons across tunneling barriers. The orbital $|n\rangle$ possess the on-site energy E_n which could be extracted from experimental spectroscopy data to describe a specific setup. In our model, the influence of the external field, specified by the harmonic driving

$$f(t) = A\cos(\Omega t) \ , \quad (3.2)$$

renders the site energies time-dependent. The field amplitude A having the dimension of an energy varies as a function of the length of the wire. It corresponds in terms of the molecular wires to the electrical field strength along the axis of lateral expansion, *i.e.*, along the electrode–electrode axis multiplied by the electron charge and again the distance of neighboring sites. For coupled quantum dots, the electrical field strength is replaced by the microwave amplitude of an oscillating gate voltage. Moreover, the driving couples to the site $|n\rangle$ scaled by the factor

$$x_n = \frac{1}{2}(N + 1 - 2n) \quad (3.3)$$

which has been chosen such that the difference between adjacent sites is always one.

The electric dipole approximation is well justified if the wavelength of the driving field is much larger than the spatial extension of the nanoconductor because the propagation of the electromagnetic field can be disregarded (Pellegrini, 1993). For both quantum dots and molecular wires investigated here,

this condition is fulfilled. Typical length and energy scales will be provided in the corresponding chapters.

3.1.2. Decomposition into Floquet basis

A further prerequisite to keep our approach feasible within the Floquet ansatz is the assumption of energy-independent lead–wire coupling. The solution of a time-periodic problem is based on the work of Floquet (1883) who developed a method to solve linear ordinary differential equations with periodic coefficients. The discrete time translation symmetry due to a periodic potential allows the separation of the solution of the wave function into a phase factor and a time-periodic contribution. As mentioned earlier, the equation of motion (2.22) for $G(t,t')$ represents an integro-differential equation. Employing the wide-band limit $\Gamma_\ell(t) = \Gamma_\ell \delta(t)$ hence yields an ordinary differential equation. In order to go beyond the wide-band limit, the retarded Green functions could be expanded within Floquet theory in terms of matrix continued fractions (Martinez, 2003; Arrachea, 2005). However, the convergence of the matrix continued fractions has to be assured, which is a difficult task (Martinez, 2005).

Solving the dynamics of the reduced system for the retarded Green function is equivalent to computing the solution for the Schrödinger-type equation

$$i\hbar \frac{d}{dt} |\Psi(t)\rangle = \left(\mathcal{H}_{\text{wire}}(t) - i\Sigma\right) |\Psi(t)\rangle \ . \tag{3.4}$$

As a consequence of the wide-band limit the real part of the self energy caused by the coupling to the leads vanishes. Hence, no renormalization in terms of a shift of the wire energies as discussed after Eq. (2.26) is present, but the imaginary part of the self-energy, which is given by

$$\Sigma = |1\rangle \frac{\Gamma_{\text{L}}}{2} \langle 1| + |N\rangle \frac{\Gamma_{\text{R}}}{2} \langle N| \ , \tag{3.5}$$

broadens the energy levels of the wire.

According to the Floquet theorem, a complete set $\{|\Psi_\alpha(t)\rangle\}$ of solutions of the linear time-dependent Eq. (3.4) with periodic coefficients can be stated

as

$$|\Psi_\alpha(t)\rangle = e^{-i(\epsilon_\alpha/\hbar - \gamma_\alpha)t}|\phi_\alpha(t)\rangle \tag{3.6}$$

with the time-periodic Floquet states $|\phi_\alpha(t)\rangle = |\phi_\alpha(t+\mathcal{T})\rangle$, which are also denoted as Floquet modes, and the complex quasienergies $\epsilon_\alpha - i\hbar\gamma_\alpha$ in analogy to Bloch theory (see Ashcroft and Mermin, 1976, chapter 8). By inserting this ansatz into (3.4), it can be easily verified that it solves this equation. It is worthwhile to note that this ansatz separates time scales. The long-time behavior is governed by the exponential phase factor, whereas the time span of one driving period is governed by the Floquet modes. Owing to their time-periodicity, we can decompose the Floquet states into a Fourier series

$$|\phi_\alpha(t)\rangle = \sum_{k=-\infty}^{\infty} e^{-ik\Omega t}|\phi_{\alpha k}\rangle \ , \tag{3.7}$$

$$|\phi_{\alpha k}\rangle = \frac{1}{\mathcal{T}}\int_0^{\mathcal{T}} dt\, e^{ik\Omega t}|\phi_\alpha(t)\rangle \ . \tag{3.8}$$

The index k is often referred to as the sideband or Floquet index. In correspondence with Bloch theory, there exist an infinite number of solutions on equal footing with ϵ_α and $|\phi_\alpha(t)\rangle$ related by the replacement

$$\epsilon_\alpha \to \epsilon_\alpha + k_\alpha\hbar\Omega \ , \qquad |\phi_\alpha(t)\rangle \to e^{ik_\alpha\Omega t}|\phi_\alpha(t)\rangle \tag{3.9}$$

with $k_\alpha = \pm 1, \pm 2, \ldots$ These classes of solutions marked by the set of indices $\{k_\alpha\}$ are physically equivalent. To identify a unique set of states it is sufficient to select those Floquet modes whose real quasienergies are situated within an energy range of $\hbar\Omega$. Thus, we can restrict ourself to the energies

$$\frac{-\hbar\Omega}{2} \leq \epsilon_\alpha < \frac{\hbar\Omega}{2} \tag{3.10}$$

also called *first Brillouin zone*. Within this range there are the same number of Floquet states as for the static, *i.e.*, undriven, system which is the number of sites N corresponding to the dimension of the configuration Hilbert space of the wire.

Now we are able to reformulate the originally time-dependent problem in terms of a stationary problem in a Hilbert space extended by the periodic

time coordinate. The corresponding eigenvalue equation, also called Floquet equation (Shirley, 1965), has the form

$$\left(\mathcal{H}_{\text{wire}}(t) - i\Sigma - i\hbar\frac{d}{dt}\right)|\phi_\alpha(t)\rangle = (\epsilon_\alpha - i\hbar\gamma_\alpha)|\phi_\alpha(t)\rangle \ . \tag{3.11}$$

The operator defined by the bracket on the left-hand side denotes the Floquet Hamiltonian which is an operator in the composite Hilbert space $\mathbb{R}\otimes\mathbb{T}$ as well as the Floquet modes $|\phi_\alpha(t)\rangle$ are eigenvectors of this Hilbert space first noted by Sambe (1973). As indicated earlier, this solution is not unique. Also

$$|\phi_{\alpha k}(t)\rangle := e^{ik\Omega t}|\phi_\alpha(t)\rangle \tag{3.12}$$

and $\epsilon_{\alpha k} := \epsilon_\alpha + k\hbar\Omega$ as the corresponding real part of the eigenvalues solves the eigenvalue problem.

A inner product of the square integrable, $\mathcal{T}$-periodic functions within the Hilbert space $\mathbb{T}$ is defined by

$$(u, v) := \frac{1}{\mathcal{T}}\int_0^{\mathcal{T}} dt\, u^*(t)v(t) \ . \tag{3.13}$$

The complete set of basis functions spanning the temporal space is given by the Fourier vectors $e^{-ik\Omega t}$, where

$$\frac{1}{\mathcal{T}}\int_0^{\mathcal{T}} dt\, e^{i(k-k')\Omega t} = \delta_{kk'} \tag{3.14}$$

denotes the condition of orthonormality. Likewise, the vectors $|\psi\rangle$ of the configuration space $\mathbb{R}$ possess the usual inner vector product $\langle\psi'|\psi\rangle$. Let us assume, there exists a complete and countable set $\{|n\rangle\}$ of states which obey

$$\langle n|n'\rangle = \delta_{nn'} \ , \qquad \sum_n |n\rangle\langle n| = \mathbb{1} \ , \tag{3.15}$$

where the unity operator $\mathbb{1}$ acts upon the configuration space $\mathbb{R}$.

Therefore combining the temporal and configuration Hilbert space, a inner product in the composite Hilbert space is set up via the relation

$$\langle\langle\phi'|\phi\rangle\rangle := \frac{1}{\mathcal{T}}\int_0^{\mathcal{T}} dt\, \langle\phi'(t)|\phi(t)\rangle \ , \tag{3.16}$$

where the notation $|\phi\rangle\rangle$, introduced by Sambe (1973) for the elements of $\mathbb{R} \otimes \mathbb{T}$, has been used. The double bracket means integration over one driving period and over all configuration space. Generally, the Floquet modes are only mutually orthogonal at equal times. In order to state the completeness relation, we need the adjoint eigenstates. However, for the non-Hermitian Floquet Hamiltonian defined by the eigenvalue equation (3.11), the (right) eigenvectors $|\phi_\alpha(t)\rangle$ are not mutually orthogonal. We also have to solve the Floquet equation for the adjoint Hamiltonian $\mathcal{H}_{\text{wire}}(t) + i\Sigma$. The corresponding eigenvalue equation reads

$$\left(\mathcal{H}_{\text{wire}}(t) + i\Sigma - i\hbar\frac{d}{dt}\right)|\chi_\alpha(t)\rangle = (\epsilon_\alpha + i\hbar\gamma_\alpha)|\chi_\alpha(t)\rangle \ , \tag{3.17}$$

where $|\chi_\alpha(t)\rangle$ denotes the left eigenvectors. The left and right Floquet modes now form at biorthogonal basis at equal times t (Morse and Freshbach, 1953, chapter 7):

$$\langle\chi_\alpha(t)|\phi_\beta(t)\rangle = \delta_{\alpha\beta} \ , \qquad \sum_\alpha |\phi_\alpha(t)\rangle\langle\chi_\alpha(t)| = \mathbb{1} \ . \tag{3.18}$$

This allows us to construct the propagator $U(t,t')$ already introduced after Eq. (2.22) which can be expressed now in terms of the left and right eigenvectors

$$U(t,t') = \sum_\alpha e^{-i(\epsilon_\alpha/\hbar - i\gamma_\alpha)(t-t')}|\phi_\alpha(t)\rangle\langle\chi_\alpha(t')| \ , \tag{3.19}$$

where the sum runs over all Floquet states within one Brillouin zone. The initial condition $U(t,t) = \mathbb{1}$ is ensured by the completeness (3.18) of the Floquet states. Therefore, the Fourier coefficients of the retarded Green function have the form

$$G^{(k)}(\epsilon) = -\frac{i}{\hbar}\int_0^{\mathcal{T}}\frac{dt}{\mathcal{T}}e^{ik\Omega t}\int_0^\infty d\tau\, e^{i\epsilon\tau/\hbar}U(t,t-\tau) \tag{3.20}$$

$$= \sum_{\alpha,k'}\frac{|\phi_{\alpha,k'+k}\rangle\langle\chi_{\alpha,k'}|}{\epsilon - (\epsilon_\alpha + k'\hbar\Omega - i\hbar\gamma_\alpha)} \ . \tag{3.21}$$

Hence, solving the eigenvalue problem defined by (3.11) and its adjoint counterpart (3.17), the current and the noise power are fully determined.

3.1.3. Numerical methods

There exists a wealth of methods to actually compute the Floquet states and complex quasienergies (see e.g., Grifoni and Hänggi, 1998, and references therein). Since we set up an eigenvalue problem in the previous section, the natural choice to compute the solution is by means of direct diagonalization. This method is not suited for systems with a fairly large number of wire sites due to the fact that a sufficiently large cut-off for the sideband index k determining basically the size of involved matrices is required to assure convergence. However, coherently coupled quantum dots and simple molecules are well within the scope of our approach.

In the following, we will expand the Floquet modes in terms of the set $\{|u_{nk}\rangle\rangle\}$ of orthonormal basis states defined by

$$|u_{nk}(t)\rangle := e^{-ik\Omega t}|n\rangle \quad . \tag{3.22}$$

The Fourier coefficients of the right Floquet modes $|\phi_\alpha(t)\rangle$ of this decomposition into the basis vectors might be written as

$$c_{nk\alpha} = \langle\langle u_{nk}|\phi_\alpha\rangle\rangle = \langle n|\phi_{\alpha k}\rangle \quad . \tag{3.23}$$

The last equality is readily verified using Eq. (3.8). A corresponding expression is obtained for the left Floquet states $|\chi_\alpha(t)\rangle$. The representation free Floquet Hamiltonian belonging to the eigenvalues $\epsilon_\alpha - i\hbar\gamma_\alpha$ is assumed to have the general form

$$H_{\mathrm{F}}(t) = H_0 + \sum_{l=1}^{\infty} A_l \cos(l\Omega t + \varphi_l) H_l - i\Sigma - i\hbar\frac{d}{dt} \quad . \tag{3.24}$$

Here, we separated the contributions of the wire Hamiltonian into its static part H_0 and a term taking care of the driving. Note that the most general form of driving has been assumed including higher harmonics—not only the first one—as well as arbitrary phase shifts φ_l. Expanding the Floquet equation into the basis states (3.22) and employing the orthogonality conditions (3.14) and (3.15), we arrive at the very compact matrix representation

$$\sum_{n',k'} H^{kk'}_{nn'} c_{n'k'\alpha} = (\epsilon_\alpha - i\hbar\gamma_\alpha) c_{nk\alpha} \quad , \tag{3.25}$$

where the matrix elements of the Floquet Hamiltonian are defined as

$$H^{kk'}_{nn'} = \left[\langle n|H_0|n'\rangle - k\hbar\Omega\delta_{nn'} - \frac{i}{2}\left(\Gamma_{\mathrm{L}}\delta_{1n}\delta_{1n'} + \Gamma_{\mathrm{R}}\delta_{Nn}\delta_{Nn'}\right)\right]\delta_{kk'} + \sum_{l=1}^{\infty}\frac{A_l}{2}\langle n|H_l|n'\rangle\left(\delta_{k,k'-l}e^{i\varphi_l} + \delta_{k,k'+l}e^{-i\varphi_l}\right) \quad . \tag{3.26}$$

The matrix elements associated with the left eigenstates are obtained upon complex conjugation. Hence in order to solve the Floquet eigenvalue problem the Fourier coefficients of the left and right Floquet modes have to be evaluated. The numerical effort reduces, however, in case of vanishing phase shifts, $\varphi_l = 0$. Then, $H_{\mathrm{F}}(t)$ is symmetric and the relation

$$\langle n|\phi_{\alpha k}\rangle = \langle\chi_{\alpha k}|n\rangle \tag{3.27}$$

holds (Morse and Freshbach, 1953, p. 886). As a consequence, only one type of coefficients has to be computed. Generally, the Floquet matrix (3.26) is band-diagonal. Most of our calculations are restricted to harmonic driving which means all contribution with $l > 1$ vanish. Hence, solely diagonal and first off-diagonal elements are present.

3.2. Fundamental symmetries

As a consequence of the discrete time translation symmetry $t \to t + \mathcal{T}$, a complete set of solutions given by the Floquet states has been already reduced to states in one Brillouin zone. The numerical effort can be further minimized exploiting additional symmetries of the system Hamiltonian $H(t)$. Furthermore, the breaking of certain symmetries, for instance, by means of a small phase shift, constitutes an excellent test for the implemented numerics. The average current depends sensitively on the phase shift for driving with higher harmonics (Lehmann et al., 2003b). Note that the breaking of symmetries is required to observe pump and ratchet effects (Reimann et al., 1997; Linke et al., 1999; Flach et al., 2000; Reimann, 2002). The basic idea behind a ratchet is that due to some spatial asymmetry an average current as a response to an alternating external field occurs although

no net bias is applied. According to the principle of Curie (1894), there is always a current present unless it is prevented by some symmetry.

In the following we characterize the relevant symmetry transformations for systems driven by a dipole field. For ease of notation, the tight-binding basis is replaced for the moment by a continuous basis in position representation. This allows one to write the symmetry transformations in a more general form also avoiding the distinction between lead and wire states. Discussing the implications on the transmission probabilities of transport processes, we will refer nevertheless again to the tight-binding basis since this involves G_{1N} and G_{N1}. Hence, we make a step back and consider the full Hamiltonian (2.1) including the lead states. The corresponding Floquet equation incorporating the dipole force $xf(t)$ due to the external field (Cohen-Tannoudji et al., 1992) has the from

$$H_{\mathrm{F}}(x,t)\phi_\alpha(x,t) = \epsilon_\alpha \phi_\alpha(x,t) \tag{3.28}$$

with the Floquet Hamiltonian

$$H_{\mathrm{F}}(x,t) = H_0(x) + xf(t) - i\hbar\frac{d}{dt} \ . \tag{3.29}$$

The contributions of the leads and the tunneling contacts are included in the static part $H_0(x)$ here and therefore no self-energy is present. Accordingly, the Fourier coefficients (3.8) read in position space

$$\phi_{\alpha k}(x) = \frac{1}{\mathcal{T}}\int_0^{\mathcal{T}} dt\, e^{ik\Omega t}\phi_\alpha(x,t) \ . \tag{3.30}$$

Note that since we are operating on the composite Hilbert space $\mathbb{R}\otimes\mathbb{T}$, we have to consider the effect of transformations on both the position and the time in order to find symmetries which yield the Floquet equation with the harmonic driving $f(t)$ invariant.

A Hamiltonian $H(t)$ is invariant under an unitary symmetry operation $\mathcal{S}$ if they commute: $[\mathcal{S}, H(t)] = 0$. The corresponding Schrödinger-like equation for the transformed propagator $\tilde{U}(t,t') = \mathcal{S}^\dagger U(t,t')\mathcal{S}$ reads

$$\pm i\hbar\frac{d}{dt}\tilde{U}(t,t') = H(t)\tilde{U}(t,t') \ , \tag{3.31}$$

where the minus sign applies for symmetry operations involving time-inversion. Formally integrating the equation and then comparing it to the equivalent expression for $U(t,t')$ results in the following condition for the Green function

$$\langle x|\tilde{U}(t,t')|x'\rangle = \langle x|\mathcal{S}^{\dagger}U(t,t')\mathcal{S}|x'\rangle = \langle x|U(t,t')|x'\rangle^{(*)} \ , \tag{3.32}$$

Note that in case of time-inversion the complex conjugation put in brackets has to be executed as a consequence of the minus sign in Eq. (3.31): $\langle x|U(t,t')|x'\rangle^* = \langle x'|U(t',t)|x\rangle$. If the condition (3.32) is fulfilled, a scattering process and its symmetric counterpart possess the same transition probability which means they are equally likely. This statement will become clearer illustrating certain symmetries below. It is important to mention that $\mathcal{S}|x'\rangle \neq |x\rangle$ is required, otherwise the two scattering processes are identical.

3.2.1. Time-reversal symmetry

Although an explicit time-dependence in the Hamiltonian breaks in general time-reversal symmetry, this is not the case for sinusoidal driving. In order to leave the Floquet Hamiltonian invariant under the time-inversion

$$\mathcal{S}_{\mathrm{T}} : (x,t) \to (x,-t) \ , \tag{3.33}$$

the condition $H_{\mathrm{F}}(x,t) = H_{\mathrm{F}}^*(x,-t)$ has to be fulfilled. For this symmetry the Floquet modes must obey $\phi_\alpha(x,t) = \phi_\alpha^*(x,-t)$ which means

$$\phi_{\alpha k}(x) = \phi_{\alpha k}^*(x) \tag{3.34}$$

for the corresponding Fourier decomposition. Therefore the Fourier coefficients are real which helps to decrease the numerical effort. In terms of the propagator, time-reversal symmetry yields according to Eq. (3.32) the condition

$$\langle 1|U(t,t')|N\rangle = \langle N|U(-t',-t)|1\rangle \ . \tag{3.35}$$

Note that we made here the transition to the discrete tight-binding basis. Writing the Fourier representation of these Green functions by employing the definition (3.20), we obtain $G_{1N}^{(k)}(\epsilon) = G_{N1}^{(-k)}(\epsilon + k\hbar\Omega)$. Therefore, the

relation of the transmission functions for two scattering events with equal probability is given by

$$T_{\mathrm{RL}}^{(k)}(\epsilon) = T_{\mathrm{LR}}^{(-k)}(\epsilon + k\hbar\Omega) \ . \tag{3.36}$$

To illustrate this, the two processes which are associated with each other by the time-reversal symmetry are depicted in Fig. 3.1(a).

3.2.2. Time-reversal parity

The combination of time-inversion and parity transformations allows to check for the so-called time-reversal symmetry defined by the operator

$$\mathcal{S}_{\mathrm{TP}} = \mathcal{S}_{\mathrm{T}}\mathcal{S}_{\mathrm{P}} : (x,t) \to (-x,-t) \ . \tag{3.37}$$

The Floquet Hamiltonian is invariant under the transformation $\mathcal{S}_{\mathrm{TP}}$ in case of $H_{\mathrm{F}}(x,t) = H_{\mathrm{F}}^{*}(-x,-t)$ and for the Floquet coefficients the condition

$$\phi_{\alpha k}(x) = \phi_{\alpha k}^{*}(-x) \tag{3.38}$$

must hold. Important to note here is the fact that our Floquet equation obeys the time-reversal symmetry if two things come together. In the first place the driving must be an odd function which implies $f(t) = -f(-t)$ and secondly $H_0(x)$ has to be invariant under space-inversion $x \to -x$, *i.e.*, $H_0(x) = H_0(-x)$. Then, the two additional minus signs acquired by the transformation $\mathcal{S}_{\mathrm{TP}}$ compensate for each other. However, a spatial symmetry in the static part $H_0(x)$ requires, in terms of the reduced system dynamics, that the lead–wire coupling is symmetric, $\Gamma_{\mathrm{L}}(\epsilon) = \Gamma_{\mathrm{R}}(\epsilon)$.

In the tight-binding basis the effect of the parity operator is described by $\mathcal{S}_{\mathrm{P}} : (q\mathrm{L}, n) \leftrightarrow (q\mathrm{R}, N-n+1)$, where $n = 1, \ldots, N$ denotes the wire states and qL, qR states in the left and right lead, respectively. The condition for the transition amplitude of equally likely scattering events related by time-reversal parity reads

$$\langle 1|U(t,t')|N\rangle = \langle 1|U(-t',-t)|N\rangle \tag{3.39}$$

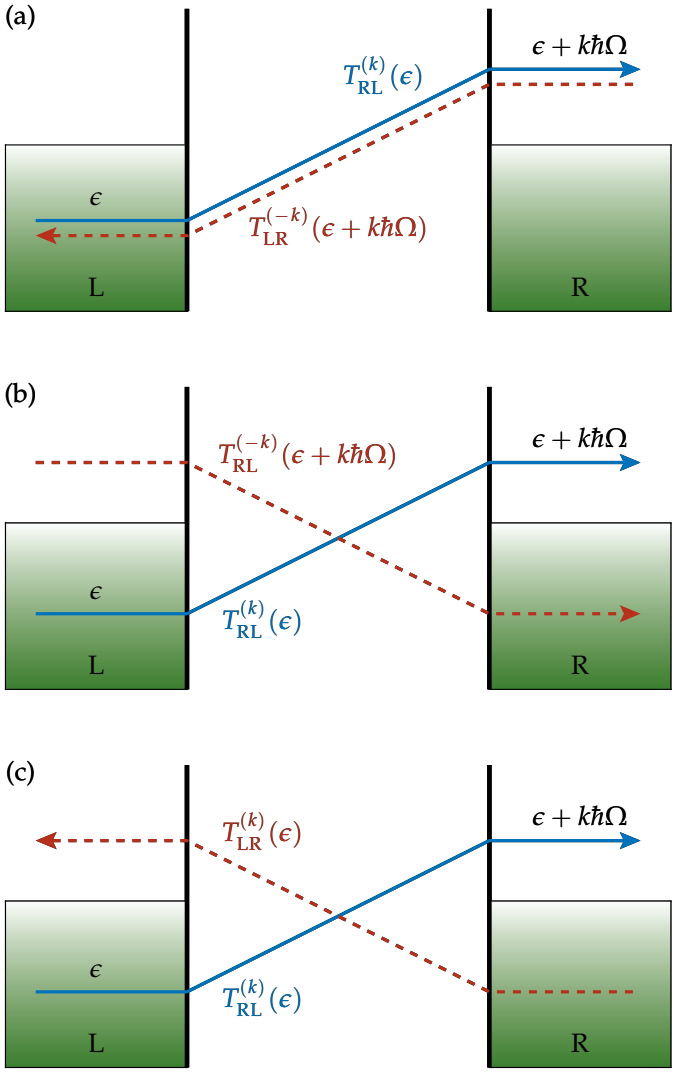

Figure 3.1: Scattering processes indicated by solid and dashed lines related to each other by certain symmetries. The two processes occur each with equal transmission probability. Depicted is (a) the time-reversal symmetry, (b) the time-reversal parity and (c) the generalized parity.

and the Fourier representation yields $G_{1N}^{(k)}(\epsilon) = G_{1N}^{(-k)}(\epsilon + k\hbar\Omega)$. The corresponding scattering processes are sketched in Fig. 3.1(b); for the transmission probability we obtain

$$T_{\mathrm{RL}}^{(k)}(\epsilon) = T_{\mathrm{RL}}^{(-k)}(\epsilon + k\hbar\Omega) \ . \tag{3.40}$$

Lehmann et al. (2003b) discussed the subtle role of time-reversal parity for different wire–lead couplings. They found within their master equation approach that for systems subject to harmonic driving and satisfying the time-reversal parity, the dc current obeys $\bar{I} \propto \Gamma^2$ for $\Gamma \to 0$, while it is generally of the order Γ for broken time-reversal symmetry.

3.2.3. Generalized parity

If the driving field obeys $f(t) = -f(t + \mathcal{T}/2)$, the Floquet Hamiltonian is invariant upon the so-called generalized parity

$$\mathcal{S}_{\mathrm{GP}} = \mathcal{S}_{\mathrm{G}}\mathcal{S}_{\mathrm{P}} : (x,t) \to (-x, t + \mathcal{T}/2) \ . \tag{3.41}$$

The time is shifted by half a period and the position is subject to parity. Here, the Floquet Hamiltonian has to satisfy $H_{\mathrm{F}}(x,t) = H_{\mathrm{F}}^*(-x, t + \mathcal{T}/2)$. Applying the transformation on the Floquet modes demonstrates that they are either even or odd under this symmetry, $\mathcal{S}_{\mathrm{GP}}\,\phi_\alpha(x,t) = \pm\phi_\alpha(x,t)$. Here we used that $\mathcal{S}_{\mathrm{GP}}^2 = 1$. As a consequence, also the Fourier coefficients can be classified by even and odd functions,

$$\phi_{\alpha k}(x) = \pm(-1)^k \phi_{\alpha k}^*(-x) \ . \tag{3.42}$$

Similar to the time-reversal parity, for generalized parity to hold the wire–lead coupling has to be symmetric too. For the corresponding process with identical likelihood, the condition (3.32) yields

$$\langle 1|U(t,t')|N\rangle = \langle N|U(t + \mathcal{T}/2, t' + \mathcal{T}/2)|1\rangle \ . \tag{3.43}$$

After deploying the Fourier decomposition, we find $G_{1N}^{(k)}(\epsilon) = G_{N1}^{(k)}(\epsilon)$, and the transversing of electrons obeying generalized parity is characterized by

$$T_{\mathrm{RL}}^{(k)}(\epsilon) = T_{\mathrm{LR}}^{(k)}(\epsilon) \ . \tag{3.44}$$

The related events are depicted schematically in Fig. 3.1(c).

With the help of this symmetry, the quasienergy spectra of superlattices exposed to laser radiation can be characterized as done by Holthaus (1992b). It also explains the degeneracy of quasienergies for tunneling in bistable potentials (Großmann et al., 1991).

4. Rotating-wave approximation

Studying the case of high-frequency driving enables one to gain a deeper insight into intriguing effects like the coherent suppression of tunneling in two-level systems (Großmann and Hänggi, 1992), superlattices (Holthaus, 1992a), and double-well heterostructures (Wagner, 1995). In the high-frequency regime a separation of time scales between the inherent tunneling dynamics of the conductor and the external force field occurs. Employing this feature allows us to solve the ac driven problem analytically by an approximate reduction to a time-independent system.

First, we will recapitulate the basic idea behind the coherent destruction of tunneling (CDT). This phenomena was first investigated by Grossmann et al. (1991) for closed systems in the context of tunneling in a bistable potential driven by an intense monochromatic field. Subsequently, we will derive a perturbation scheme based on Floquet theory which is applicable for high-frequency driving. Resonant transitions can be also treated as long as only one basic resonance frequency is involved. The case of arbitrary many levels with identical on-site energies—no internal resonances are present then—might be denoted within our approach formally as the zeroth resonance. Hence, the method we introduce in this chapter can be interpreted in the spirit of the familiar rotating-wave approximation (RWA) of Rabi et al. (1954). However, a novel aspect here is the consistent incorporation of environmental degrees of freedom like the coupling to the leads (Kohler, Camalet, Strass, Lehmann, Ingold, and Hänggi, 2004;Strass et al., 2005b). In addition, this approximation scheme is not limited to a small field coupling in contrast to the traditional RWA, *i.e.*, it is valid for arbitrary driving amplitude A under the condition that the driving quanta $\hbar\Omega$ defines the largest energy scale of the problem.

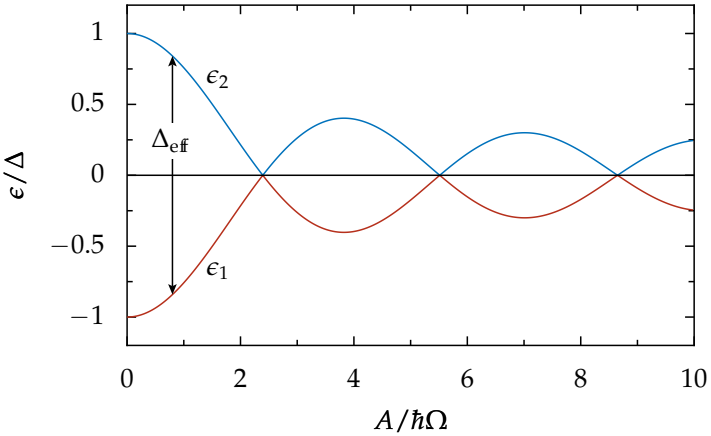

Figure 4.1: Quasienergy spectrum as a function of the driving amplitude for a unbiased two-level system, *i.e.*, identical on-site energies $E_1 = E_2 = 0$. The system is driven harmonically with angular frequency $\Omega = 10\Delta/\hbar$. Exact crossings occur whenever $J_0(A/\hbar\Omega) = 0$.

4.1. Coherent destruction of tunneling

In a double-well potential, a particle localized in one of the wells can tunnel back and forth across the central barrier characterized by the tunnel splitting which corresponds to Δ in our model. The relevant time scale for these tunneling events is given by

$$\frac{\hbar}{e_2 - e_1} = \frac{\hbar}{\Delta} \ , \tag{4.1}$$

where e_1 and e_2 denote the energies of the ground and first excited state, respectively, in the doublet. For the driven case, however, these energies have to be replaced by the quasienergies ϵ_1 and ϵ_2. As can be observed in Fig. 4.1, the spectrum of the quasienergies calculated for fast driving ($\hbar\Omega \gg \Delta$) as a function of the driving amplitude exhibits exact crossings. At these crossings, the tunneling time characterized by (4.1) diverges and consequently the tunneling dynamics comes to a standstill as the particle is totally local-

ized in one of the wells. The driven degenerate two-level system (TLS) is modeled by the Hamiltonian

$$\mathcal{H}_{\mathrm{TLS}}(t) = -\frac{\Delta}{2}\sigma_x + \frac{A}{2}\cos(\Omega t)\sigma_z \ , \tag{4.2}$$

where we used the notation in the pseudo-spin basis denoted by the Pauli matrices $\sigma_x = |1\rangle\langle 2| + |2\rangle\langle 1|$ and $\sigma_z = |1\rangle\langle 1| - |2\rangle\langle 2|$. The location of the crossings can be approximately determined by a transformation into a rotating frame which accounts for the time-dependent part of $\mathcal{H}_{\mathrm{TLS}}(t)$ and subsequently averaging over one cycle of the driving period. This corresponds to a separation of time scales and yields the static Hamiltonian

$$\mathcal{H}_{\mathrm{TLS,eff}} = -\frac{\Delta_{\mathrm{eff}}}{2}\sigma_x \tag{4.3}$$

with the renormalized tunneling matrix element $\Delta_{\mathrm{eff}} = J_0(A/\hbar\Omega)\Delta$ (Großmann and Hänggi, 1992). Here, J_0 is the zeroth order Bessel function of the first kind and the values of $A/\hbar\Omega$ for its zeros coincide with the crossings in Fig. 4.1.

4.2. Rotating-wave approximation for driven transport

Transport problems, however, imply open systems. Thus we need to extend the ideas from the preceding section and find a proper RWA treatment not only for the wire system but also for the coupling to the leads. Within Floquet theory, the time-dependent system is addressed as a eigenvalue problem with the crucial benefit that we can apply *stationary* perturbation theory in the composite Hilbert space $\mathbb{R} \otimes \mathbb{T}$. This has been asserted by Shirley (1965) and Sambe (1973). The RWA presented here is the lowest order degenerate perturbation theory in the sense that the zeroth order Floquet states and the first order quasienergies are involved.

As a starting point, we consider the static part of the wire Hamiltonian as a perturbation. Therefore, let us assume the single-particle Hamiltonian (3.1) can be written as follows:

$$\mathcal{H}_{\mathrm{wire}}(t) = \mathcal{H}_0 + \mathcal{H}_1 f(t) \ , \tag{4.4}$$

where $\mathcal{H}_1 = \sum_n x_n |n\rangle\langle n|$ and $\mathcal{H}_0 = \mathcal{H}_0^{'} + \mathcal{H}_0^{''}$. Thereby, the separation of the static Hamiltonian $\mathcal{H}_0$ into the two contributions $\mathcal{H}_0^{'}$ and $\mathcal{H}_0^{''}$ has to be chosen such, that

$$\mathcal{H}_0^{''} = \sum_n r_n \hbar\Omega |n\rangle\langle n| \ , \tag{4.5}$$

where $r_n = 0, \pm 1, \pm 2, \ldots$, while all matrix elements of $\mathcal{H}_0^{'}$ are assumed to be much smaller than the driving quanta $\hbar\Omega$. Hence, from a physical point of view, the way $\mathcal{H}_0^{''}$ is defined implies that either all internal transitions of the wire must be close to resonance with the driving field, or have to be much smaller than $\hbar\Omega$. The latter case is formally the zeroth resonance. The situation of higher-order resonances, which might occur for large driving amplitudes, is accounted for by $r_n > 1$. If no internal resonance is present, the case $r_n = 0$ for all n applies, *i.e.*, $\mathcal{H}_0^{''} = 0$. Note that we demand in addition that solely resonant transitions emerge which are characterized by an unique angular frequency Ω.

The key point of this approximation is that the photon energy $\hbar\Omega$ of the driving field which defines the energy scale of the time-dependent Hamiltonian is much larger than the matrix elements of the static part $\mathcal{H}_0^{'}$. Hence for fast driving, the latter contribution represents a perturbation. The eigenstates of the unperturbed Floquet Hamiltonian near resonance,

$$\sum_n [r_n \hbar\Omega + x_n f(t)] |n\rangle\langle n| - i\hbar \frac{d}{dt} \ , \tag{4.6}$$

assume thus the form

$$|\phi_{nk}^{(0)}(t)\rangle = e^{-i\theta_n(t) + ik\Omega t} |n\rangle \ . \tag{4.7}$$

These eigenstates mark the zeroth order Floquet states with the quasienergies $k\hbar\Omega$ and the time-dependent phase is defined as

$$\theta_n(t) = \frac{1}{\hbar} \int_0^t dt' [r_n \hbar\Omega + x_n f(t')] \ . \tag{4.8}$$

Each k in the Floquet states defines a degenerate subspace of the composite Hilbert space. Hence, to compute the first-order correction of the Floquet

states and quasienergies, we can restrict ourselves to the subspace defined by $k = 0$ for which the zeroth order quasienergies are equal to zero. This subspace is complete in the sense that it contains all physically distinct Floquet modes. In order to obtain a perturbative solution including the self-energy Σ, we have to solve the time-independent eigenvalue equation

$$\left(\mathcal{H}_{\text{eff}} - i\Sigma\right)|\psi_\alpha\rangle = \left(\epsilon_\alpha^{(1)} - i\hbar\gamma_\alpha^{(1)}\right)|\psi_\alpha\rangle \ . \tag{4.9}$$

The effective Hamiltonian $\mathcal{H}_{\text{eff}}$ is defined by the matrix elements of the static tunneling Hamiltonian $\mathcal{H}_0^{'}$ with the unperturbed states (4.7) to read

$$(\mathcal{H}_{\text{eff}})_{nn'} = \frac{1}{\mathcal{T}}\int_0^{\mathcal{T}} dt\, \langle\phi_n^{(0)}(t)|\mathcal{H}_0^{'}|\phi_{n'}^{(0)}(t)\rangle \ . \tag{4.10}$$

Having a closer look at the degenerate perturbation theory, we remark that as a result of the time integral, the quasienergies $\epsilon_\alpha^{(1)} - i\hbar\gamma_\alpha^{(1)}$ are obtained to first order in $1/\Omega$ when solving the time-independent eigenvalue problem (4.9). The corresponding perturbed Floquet state can be written as

$$|\phi_\alpha(t)\rangle = U_0(t)|\psi_\alpha\rangle \tag{4.11}$$

with the unitary transformation

$$U_0(t) = \sum_n e^{-i\theta_n(t)}|n\rangle\langle n| \ . \tag{4.12}$$

The time-dependent phase factor (4.8) is $\mathcal{T}$-periodic,

$$e^{-i\theta_n(t)} = e^{-i\theta_n(t+\mathcal{T})} \ , \tag{4.13}$$

and, thus, the operator $U_0(t) = U_0(t+\mathcal{T})$ also satisfies the time-periodicity of the external field. Consequently, the exponential function (4.13) can be expanded into the Fourier series

$$e^{-i\theta_n(t)} = \sum_k a_{nk}e^{-ik\Omega t} \ , \tag{4.14}$$

$$a_{nk} = \frac{1}{\mathcal{T}}\int_0^{\mathcal{T}} dt\, e^{ik\Omega t}e^{-i\theta_n(t)} \ . \tag{4.15}$$

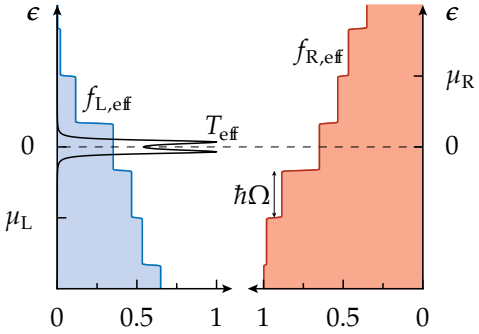

Figure 4.2: Typical energy-dependence of the renormalized transmission function $T_{\text{eff}}(\epsilon)$ and the effective electron distributions $f_{\ell,\text{eff}}(\epsilon)$ for a two-site system harmonically driven in the high-frequency regime. The step transitions in $f_{\ell,\text{eff}}(\epsilon)$ are smeared out depending on the temperature, while the step width corresponds to the driving quanta $\hbar\Omega$.

Upon inserting the Floquet states (4.11) into the definition (3.8) of the Fourier coefficients, we find $\langle n|\phi_{\alpha k}\rangle = a_{nk}\langle n|\psi_\alpha\rangle$. Hence when compared with the retarded Green function (3.21) for arbitrary driving, we note that within the presented approximation the retarded Green function can be expressed as

$$G^{(k)}_{nn'}(\epsilon) = \sum_{k'} a_{n,k+k'} a_{n'k'} G^{\text{eff}}_{nn'}(\epsilon - k'\hbar\Omega) \ , \tag{4.16}$$

where

$$G^{\text{eff}}(\epsilon) = \sum_\alpha \frac{|\psi_\alpha\rangle\langle\psi^\dagger_\alpha|}{\epsilon - \epsilon^{(1)}_\alpha + i\hbar\gamma^{(1)}_\alpha} \tag{4.17}$$

denotes the retarded Green function which solves the time-independent eigenvalue problem (4.9). Here, the adjoint state $|\psi^\dagger_\alpha\rangle$ corresponds to the left Floquet states $|\chi_\alpha(t)\rangle$ introduced in chapter 3.

In order to evaluate the dc current (2.36) in the wide-band limit, we apply the sum rule

$$\sum_{k'} a_{n,k+k'} a^*_{nk'} = \delta_{k0} \ , \tag{4.18}$$

which follows from the Fourier decomposition (4.15) and shift the energy argument $\epsilon \to \epsilon + k'\hbar\Omega$ to arrive at

$$\bar{I}_{\mathrm{RWA}} = \frac{e}{h}\int d\epsilon \left[f_{\mathrm{R,eff}}(\epsilon) - f_{\mathrm{L,eff}}(\epsilon)\right] T_{\mathrm{eff}}(\epsilon) \ . \tag{4.19}$$

Comparing this approximate current formula to the outcome of the static conductor (see Appendix A), we realize that this expression is formally the same as in the time-independent case, but with the transmission function substituted with the effective transmission

$$T_{\mathrm{eff}}(\epsilon) = \Gamma_{\mathrm{L}}\Gamma_{\mathrm{R}}|G^{\mathrm{eff}}_{1N}(\epsilon)|^2 \ , \tag{4.20}$$

and with the Fermi functions replaced by the effective electron distributions

$$f_{\mathrm{L,eff}}(\epsilon) = \sum_k |a_{1k}|^2 f_{\mathrm{L}}(\epsilon + k\hbar\Omega) \tag{4.21}$$

and $f_{\mathrm{R,eff}}(\epsilon)$, respectively. The expression for the latter is obtained by interchanging $(1,\mathrm{L}) \leftrightarrow (N,\mathrm{R})$. For cosine driving for instance, the Fourier coefficients a_{nk} become Bessel functions. The effective Fermi distribution resembles not a simple step function anymore, but exhibits many steps having the width $\hbar\Omega$ weighted by the factor $|a_{1/N,k}|^2$ for the kth step. Physically, the steps can be interpreted as processes in which an electron of energy ϵ is transfered from the lead to the conducting region under absorption (emission) of $|k|$ photons for $k < 0$ ($k > 0$). The renormalized quantities are depicted for illustration for a two-site system with harmonic driving in Fig. 4.2. Note that for an unbiased system ($E_1 = E_2 = 0$), the effective transmission function is sharply peaked around $\epsilon = 0$ where the Lorentzian-like peak width is of the size $(\Gamma^2 + \Delta^2)^{1/2}$ and the effective electron distributions are thus for fast driving $\Omega \gg \Delta, \Gamma$ constant in the relevant transport energy regime.

The expression for the noise power is obtained by inserting the retarded Green function (4.16) for the high-frequency regime into the noise expression (2.40). Again employing the sum rule (4.18) and disregarding any terms with $G^{\mathrm{eff}}(\epsilon - k\hbar\Omega)G^{\mathrm{eff}}(\epsilon - k'\hbar\Omega)$ for $k \neq k'$, the noise assumes the same form as in the static case, but with the renormalized quantities $T_{\mathrm{eff}}(\epsilon)$ and

$f_{\ell,\mathrm{eff}}(\epsilon)$. One arrives at

$$\begin{aligned}\bar{S}_{\mathrm{RWA}} = \frac{e^2}{h}\int d\epsilon \Big\{ & T_{\mathrm{eff}}(\epsilon)[f_{\mathrm{L,eff}}(\epsilon)\bar{f}_{\mathrm{L,eff}}(\epsilon) + f_{\mathrm{R,eff}}(\epsilon)\bar{f}_{\mathrm{R,eff}}(\epsilon)] \\ & + T_{\mathrm{eff}}(\epsilon)[1 - T_{\mathrm{eff}}(\epsilon)][f_{\mathrm{R,eff}}(\epsilon) - f_{\mathrm{L,eff}}(\epsilon)]^2 \Big\} \ ,\end{aligned} \tag{4.22}$$

where $\bar{f}_{\ell,\mathrm{eff}} = 1 - f_{\ell,\mathrm{eff}}$.

To highlight the RWA from a different angle, it is interesting to note that the unitary transformation $U_0(t)$ defines the interaction picture of our system which means $\mathcal{H}_0^{'}$ denotes the corresponding interaction Hamiltonian. Therefore, the interaction picture of the wire Hamiltonian is defined as

$$\widetilde{\mathcal{H}}_{\mathrm{eff}}(t) = U_0^{\dagger}(t)\mathcal{H}_{\mathrm{wire}}(t)U_0(t) - i\hbar\dot{U}_0^{\dagger}(t)U_0(t) \ . \tag{4.23}$$

Note that the unitary transformation is constructed such that $\widetilde{H}(t)$ satisfies the time-periodicity of the original problem (2.1). In order to recognize its accordance with the perturbative scheme presented so far, we should note that the time-average of $\widetilde{\mathcal{H}}_{\mathrm{eff}}(t)$ over one driving period yields Eq. (4.10). Physically, it is very instructive to interpret $U_0(t)$ as a rotation of the reference frame in the spirit of the magnetic resonance interpretation of Rabi as anticipated already in Eq. (4.11). The transformation basically separates time scales between the slow tunneling dynamics and the fast oscillating Floquet modes. Hence, averaging the whole system over one driving period still reproduces the essential dynamics, but at the end of the day we are left with a time-independent problem characterized by an effective electron distribution and an effective transmission function.

5. Coherent shot noise control

As a paradigmatic effect for coherence phenomena in nanoconductors which originate from the influence of a monochromatic dipole field, we discuss in detail the setup of a two-level system (TLS) which displays coherent transport suppression. In particular, we are interested in understanding the mechanisms that contribute at the same time to a reduction of the relative noise level. Tunneling suppression in closed systems has been studied theoretically in a number of cases (Grossmann et al., 1991; Holthaus, 1992a; Wagner, 1995; Creffield and Platero, 2002). The investigation in the context of a transport setup with two leads connected to the wire, however, has been accomplished only recently by Camalet et al. (2003) within the scattering formalism presented in this work and by Lehmann et al. (2003a) within a master equation approach. Coherence effects of a great variety of systems in physics and chemistry can be described qualitatively based on the two-level model (*e.g.* Allen and Eberly, 1975; Slichter, 1996). Therefore, we focus here on a wire consisting of two sites (Kohler, Camalet, Strass, Lehmann, Ingold, and Hänggi, 2004). Beyond that, the shot noise control has been also addressed for wires comprising three (Camalet et al., 2003; Strass et al., 2005b) and four sites (Camalet et al., 2004).

A crucial requirement for the appearance of noise suppression is the fact that the on-site energies of the TLS have to oscillate relative to each other. This is achieved in our model by the dipole driving. In the case of spatially homogeneous driving in which all on-site energies are shifted equally by the external driving, the wire can be described with the theory developed by Tien and Gordon (1963). Applying a gauge transformation, the homogeneous driving can be mapped onto a system with oscillating chemical potentials in the leads while the potential inside the conductor becomes time-independent. Thus, Tien and Gordon modeled driven transport by an ac bias voltage which only modulates the energies of the electrons in the

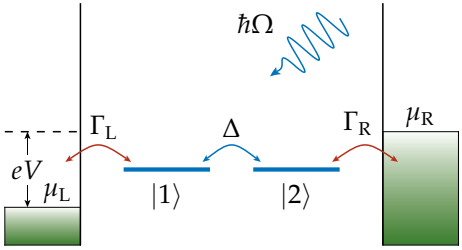

Figure 5.1: Level structure of a nanoconductor with two sites. Each site is coupled to the respective lead with chemical potentials μ_L and $\mu_R = \mu_L + eV$ and the sites are connected via the tunneling matrix element Δ. The system is driven harmonically with $f(t) \propto \cos(\Omega t)$.

leads. As an extension of this theory, the noise properties of such systems have been explored by Tucker and Feldman (1979; 1985). However, the Tien-Gordon approach is not sufficient if the internal levels oscillate with a phase lag as employed for the coherent suppression of tunneling.

5.1. Unbiased two-level system

The model system which has been already introduced briefly in the context of CDT in section 4.1 is depicted in Fig. 5.1 and the corresponding wire Hamiltonian in the localized basis $|1\rangle$ and $|2\rangle$ reads

$$\mathcal{H}_{\mathrm{TLS}}(t) = -\Delta\sigma_x + \frac{A}{2}\cos(\Omega t)\sigma_z \ . \tag{5.1}$$

The system does not possess an internal bias. To simplify the resulting expression for the current and its noise, the energy scale has been shifted such that the on-site energies are zero and the chemical potentials $\mu_R = +eV/2$ and $\mu_L = -eV/2$ define a bias voltage. It is important to note that an external bias voltage possibly shifts the on-site energies thereby creating a potential profile along the wire induced by a static dipole force (Pleutin et al., 2003; Nitzan et al., 2002). We disregard the influence of such a voltage profile because it does not alter the relevant coherence effect for a two-level system

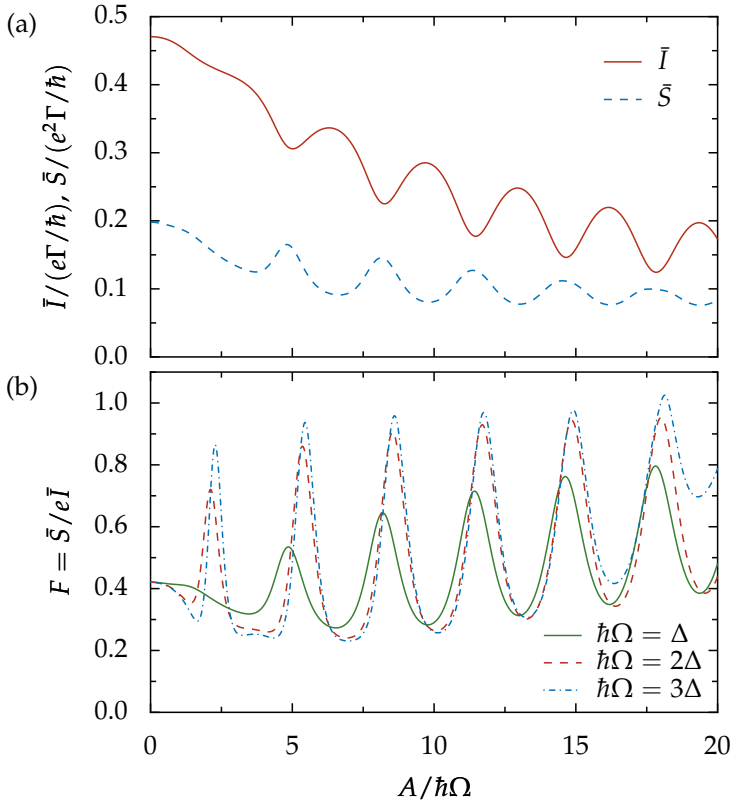

Figure 5.2: (a) Time-averaged current $\bar{I}$ (solid) and zero-frequency noise $\bar{S}$ (dashed) as a function of the driving amplitude A for driving frequency $\Omega = \Delta/\hbar$. (b) Corresponding Fano factor for different frequencies Ω. The other parameters are given by the coupling strength $\Gamma = 0.5\Delta$ and the voltage $V = 48\Delta/e$.

in a qualitative way (Lehmann et al., 2003a). Thus, a symmetric voltage drop solely at the contacts is assumed.

The dc current (2.36) and the zero-frequency noise (2.40) are calculated numerically in the zero temperature limit. This is well justified from a physical point of view because for molecular wires at room temperature and quan-

tum dots at helium temperature thermal excitations do not play a significant role. As a consequence, the Fermi functions are simple step functions. This fact spares a numerical computation of the energy integral because the retarded Green function (3.21) can be evaluated analytically once the Floquet modes and quasienergies have been determined by direct diagonalization. Figure 5.2 depicts the current and noise for relatively large voltage. Note that we assume that each site couples equally strongly to the respective lead, $\Gamma_{\mathrm{L}} = \Gamma_{\mathrm{R}} = \Gamma$. The transport for excitation energies $\hbar\Omega$, which are of the same size or somewhat larger as the resonant tunneling energies determined by Δ, is investigated. An oscillating behavior of the current and the noise as a function of the driving amplitude can be observed in Fig. 5.2(a). The dc current exhibits distinct minima accompanied by maxima for the noise and *vice versa*. For small driving frequency $\Omega = \Delta/\hbar$, the Fano factor displays only a single minimum in Fig. 5.2(b) in case of small amplitudes. The structure becomes richer for larger frequencies for which a double minimum with a notably low value ($F \approx 0.25$) appears. In addition, a shift of the minima towards smaller amplitudes occurs.

5.2. Suppression of shot noise

5.2.1. High-frequency approximation

To shed light onto the shot noise reduction characterized by the minima in the Fano factor, it is insightful to explore the high-frequency limit. We can apply therefore the RWA discussed in chapter 4. For the unbiased TLS, this high-frequency approximation denotes formally the zeroth resonance case as there is no resonant transition present. Thus, the time-dependent phase (4.8) with $r_n = 0$ for the sites $n = 1, 2$ becomes

$$\theta_n(t) = (-1)^n \frac{A}{2\hbar\Omega} \sin(\Omega t) \ . \tag{5.2}$$

Then, the coefficients a_{nk} defined by (4.15) turn out to be Bessel functions. Making use of the definition (4.10), the effective Hamiltonian describing the

driven system becomes

$$\mathcal{H}_{\mathrm{TLS,eff}} = -\Delta_{\mathrm{eff}}\,\sigma_x \ . \tag{5.3}$$

Within a high-frequency approximation, the driven two-site system (5.1) hence acts as an unbiased static system with the effective hopping matrix element

$$\Delta_{\mathrm{eff}} = J_0\left(\frac{A}{\hbar\Omega}\right)\Delta \ , \tag{5.4}$$

where J_0 is the zeroth order Bessel function of the first kind. The driving amplitude A and frequency Ω can now be chosen such that Δ_{eff} vanishes and consequently tunnelling between the two sites no longer occurs as argued for the coherent destruction of tunneling (cf. section 4.1).

Accordingly, the effective electron distributions can be evaluated and for the relevant energy regime $\epsilon = 0$ (cf. Fig. 4.2) and we obtain

$$f_{\ell,\mathrm{eff}}(0) = \sum_{k<\mu_\ell/\hbar\Omega} J_k^2\left(\frac{A}{2\hbar\Omega}\right) \ . \tag{5.5}$$

The resulting expressions for the approximate current and noise can be nicely put in terms of the static quantities in the limit of very large voltage which are stated in Appendix A. With the replacement $\Delta \to \Delta_{\mathrm{eff}}$ in (A.11) and (A.12), we denote the time-averaged current and the zero-frequency noise in this limit by $\bar{I}_\infty$ and $\bar{S}_\infty$. Substituting $f_\ell(\epsilon)$ by $f_{\ell,\mathrm{eff}}(\epsilon)$, the transport for high-frequency driving is eventually described by

$$\bar{I}_{\mathrm{RWA}} = \lambda\bar{I}_\infty = \frac{e\Gamma}{2\hbar}\frac{\lambda\Delta_{\mathrm{eff}}^2}{\Delta_{\mathrm{eff}}^2 + (\Gamma/2)^2} \ , \tag{5.6}$$

$$\begin{aligned}\bar{S}_{\mathrm{RWA}} &= \lambda^2\bar{S}_\infty + \frac{e}{2}(1-\lambda^2)\bar{I}_\infty \\ &= \frac{e^2\Gamma}{\hbar}\frac{2\lambda^2\Delta_{\mathrm{eff}}^2(\Gamma^4 - 2\Gamma^2\Delta_{\mathrm{eff}}^2 + 8\Delta_{\mathrm{eff}}^4)}{(4\Delta_{\mathrm{eff}}^2 + \Gamma^2)^3} + \frac{1-\lambda^2}{2\lambda}\,e\bar{I}_{\mathrm{RWA}} \ ,\end{aligned} \tag{5.7}$$

where

$$\lambda = f_{\mathrm{R,eff}}(0) - f_{\mathrm{L,eff}}(0) = \sum_{|k|\le K(V)} \mathrm{sgn}(V)\, J_k^2\left(\frac{A}{2\hbar\Omega}\right) \ . \tag{5.8}$$

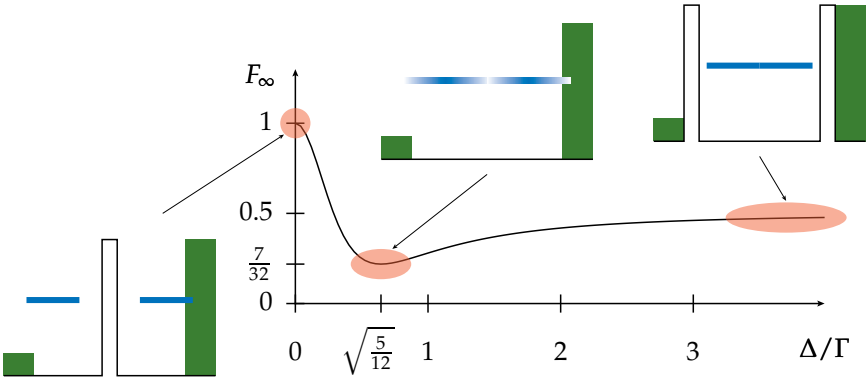

Figure 5.3: Fano factor F_∞ as a function of Δ/Γ. For $\Delta \ll \Gamma$, the bottleneck of the transport is the tunnelling process between the two sites yielding a Fano factor $F_\infty = 1$. In the opposite limit $\Delta \gg \Gamma$, we obtain transport through a double-barrier structure with a corresponding Fano factor $F_\infty = 1/2$. In the intermediate regime the Fano factor assumes a minimum at the position indicated by the special ticks in the plot.

Here, $K(V)$ is a shorthand notation for the integer part of $e|V|/2\hbar\Omega$. Note that the Fano factor $F_{\mathrm{RWA}} = \bar{S}_{\mathrm{RWA}}/e\bar{I}_{\mathrm{RWA}}$ for fixed A/Ω reaches its minimal value in the infinite voltage limit. Since $J_k(x) \approx 0$ for $x > k$ and $\sum_k J_k^2(x) = 1$, the dc current and the zero frequency noise are well approximated for $A < eV$ by their asymptotic values for infinite voltage, $\bar{I}_{\mathrm{RWA}} \approx \bar{I}_\infty$ and $\bar{S}_{\mathrm{RWA}} \approx \bar{S}_\infty$. We remark that, in contrast to the static case, the result (5.7) contains contributions stemming from the first term in the noise expression (A.5) even in the zero-temperature limit.

In order to explain the shot noise suppression in detail, it is very helpful to discuss briefly the static case I_∞ and S_∞ stated by (A.11) and (A.12), respectively. In Fig. 5.3, the Fano factor $F_\infty = S_\infty/eI_\infty$ is depicted as a function of the ratio of the tunnelling matrix element Δ and the level width Γ. For weak wire–lead coupling $\Gamma \ll \Delta$, the two contacts between the TLS and the leads form the limiting step of the transport process. We effectively arrive at transport through a double-barrier system with a Fano factor $F_\infty = 1/2$

(Chen and Ting, 1991). On the other hand, for $\Gamma \gg \Delta$ the two sites hybridize with the adjacent lead and effectively only a single barrier remains. This yields a Fano factor $F_\infty = 1$. At the crossover between these two regimes, the channel is optimally transparent and, consequently, the Fano factor assumes a minimum. From the expression (A.13), we find the optimal hopping matrix element $\Delta = \sqrt{5/12}\,\Gamma$ yielding a minimal Fano factor of $F_\infty = 7/32$. We remark that the minimum decreases further if the number of sites in the system is increased (Camalet et al., 2003).

5.2.2. Comparison with exact results

Figures 5.4(b), (c) and (d) depict by solid lines the time-averaged current, the zero-frequency noise and the Fano factor at zero temperature obtained within our numerically exact Floquet-Green scattering formalism. Note that the particular value of $V = 48\Delta/e$ for the voltage has been selected to avoid the chemical potentials to lie closely to multiples of $\hbar\Omega$. A comparison of these numerically exact results for current and noise with the approximate expressions (5.6) and (5.7) depicted by dashed lines shows a good agreement for the parameters chosen. The agreement improves with increasing frequency: already for $\Omega = 10\Delta/\hbar$, it is found that the exact and approximate results can practically no longer be distinguished.

The exact numerical results show even stronger suppressions compared to Fig. 5.2 of both the current and the noise for certain driving amplitudes. This behavior can be explained within the high-frequency approximation: Whenever the ratio $A/\hbar\Omega$ corresponds to a zero of the Bessel function J_0, the effective hopping matrix element Δ_{eff} vanishes [cf. Fig. 5.4(a)] and consequently the current and the noise become zero. Note that the exact result exhibits still a residual current and noise. The suppressions of the current and noise lead to peaks of the Fano factor F as a function of the driving amplitude as revealed in Fig. 5.4(d). For sufficiently small driving amplitudes, these peaks are accompanied by minima which correspond to $|\Delta_{\text{eff}}| \simeq \sqrt{5/12}\,\Gamma$ indicated by the dotted line in Fig. 5.4(a).

For driving amplitudes $A \lesssim eV$, the finite voltage results (5.6) and (5.7) for the dc current and the noise strength are well described by the results

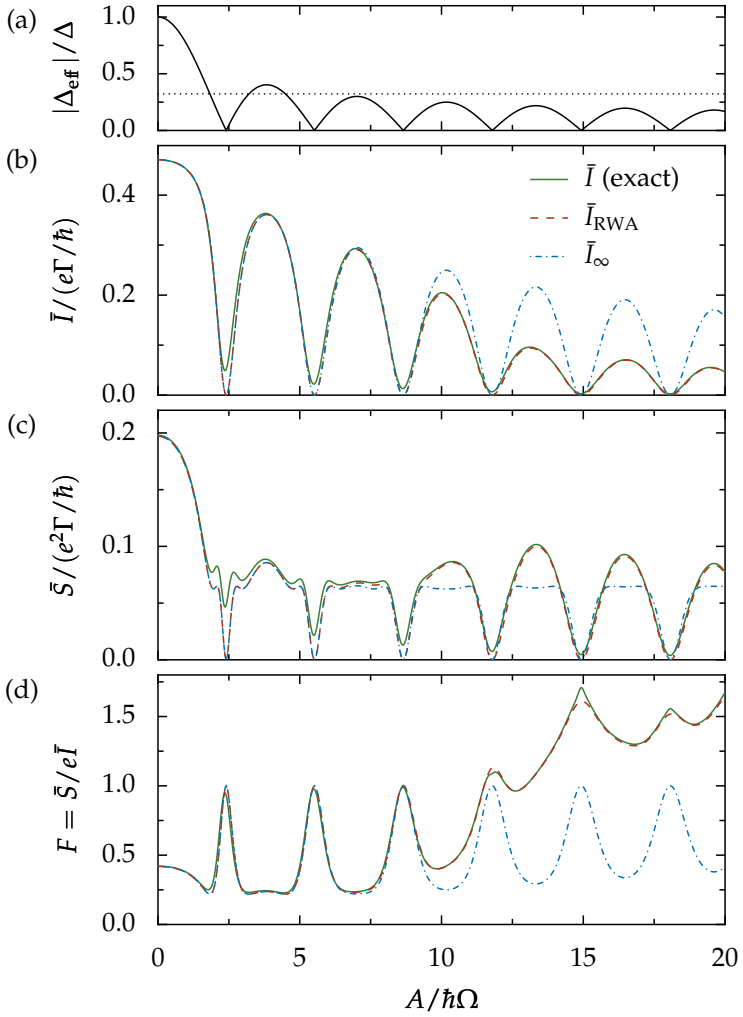

Figure 5.4: (a) Effective hopping matrix element $|\Delta_{\text{eff}}|$, (b) time-averaged current $\bar{I}$, (c) zero-frequency noise $\bar{S}$, and (d) Fano factor as a function of the driving amplitude A. Shown are the numerically exact results (solid lines), the approximative results for finite (dashed) and infinite voltage (dashed-dotted). All parameters are as in Fig. 5.2 except for $\Omega = 5\,\Delta/\hbar$. The dotted line in (a) marks the value $\sqrt{5/12}\,\Gamma$ for which the Fano factor assumes its minimum.

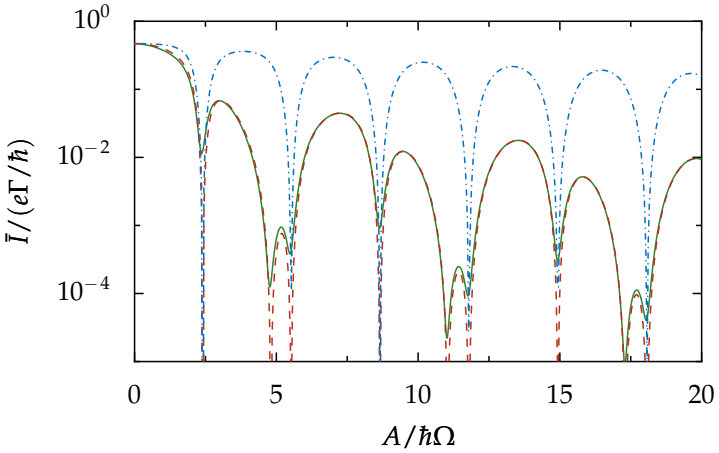

Figure 5.5: Time-averaged current $\bar{I}$ as a function of the driving amplitude A. Shown are the numerically exact result (solid line), the approximate result (5.6) for finite voltage (dashed line) and the infinite voltage result (dashed-dotted line). The coupling strength is $\Gamma = 0.5\,\Delta$, the driving frequency is $\Omega = 5\,\Delta/\hbar$, and the voltage reads $V = 5\,\Delta/e$.

(A.11) and (A.12) for infinite voltage with Δ replaced by Δ_{eff}. In this regime, the Fano factor reaches the maxima $F = 1$. In contrast, for larger driving amplitudes $A > eV$, we find a Fano factor larger than that predicted by the static expression (A.13), as already discussed below (5.8). In particular, the Fano factor can assume values $F > 1$.

Finally, we consider in Fig. 5.5 the case of intermediate voltages such that $\Delta, \Gamma < eV < 2\hbar\Omega$. Then, only the zero photon channel contributes and hence the current $\bar{I} = \bar{I}_\infty J_0^2(A/2\hbar\Omega)$ is considerably lower than that for large voltages. Now, in addition, a new type of suppression appears at twice the amplitude compared to the suppressions discussed above. The physical reason for this new kind of suppression lies in the fact that the effective distribution functions in the two leads are equal at the relevant energies and therefore no dc current can flow. Nevertheless, the noise remains finite and, consequently, the Fano factor diverges.

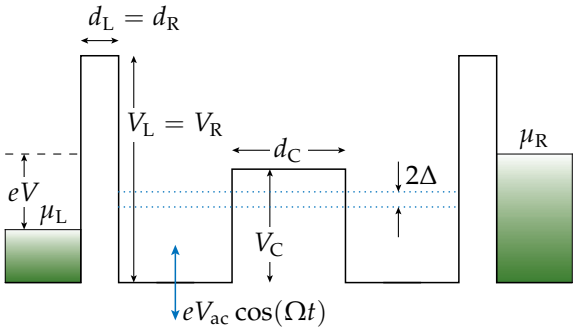

Figure 5.6: Model potential for the double-well heterostructure. In the numerical calculations, we employ barriers with the heights $V_L = V_R = 90\,\text{meV}$, $V_C = 40\,\text{meV}$ and the widths $d_L = d_R = 5\,\text{nm}$, $d_C = 15\,\text{nm}$. The dotted lines mark the energy of a metastable tunnel doublet with splitting energy 2Δ. The left well is subject to an electric dipole field generated by an alternating gate voltage with amplitude V_{ac}.

5.3. Current suppression in heterostructures

Semiconductor heterostructures represent a popular physical system for the investigation of mesoscopic transport (Beenakker and van Houten, 1991; Imry, 1997) and tunnelling phenomena (Esaki and Tsu, 1970; Tsu and Esaki, 1973; Capasso and Datta, 1990). The main reason for this is the high mobility and the rather long mean free path of the charge carriers populating them. Standard beam epitaxy techniques make the accurate growth of alloys of such materials on substrates possible, and the nearly identical lattice parameters, together with the possibility of controlling the band gap, turns the combination GaAs/AlGaAs into an ideal candidate for building complex low dimensional structures with quantum wells and tunnel barriers. Moreover, these setups open various ways to study tunnelling in time-dependent systems.

An experimental setup of a TLS can be realized by a triple-barrier structure as depicted in Fig. 5.6. The barrier heights and widths correspond to typical values in GaAs/AlGaAs heterostructures (Capasso and Datta, 1990).

Note that in contrast to the model (5.1), the driving acts solely on one well, while the other one remains unaffected by the external field. A standard approach to investigate theoretically the tunneling currents in such systems is the transfer-matrix method. Within this method, the Floquet states are decomposed into plane waves throughout the driven heterostructure, so that they can be appropriately matched with the inelastic scattering channels in the leads characterized by $E + k\hbar\Omega$. This decomposition allows to separate the time- and the space-dependent parts of the wave function. For a spatially constant potential with a time-dependent gate voltage $V_{\mathrm{ac}}(t) = V_{\mathrm{ac}} \cos(\Omega t)$, the solution of the Schrödinger equation is readily obtained to read

$$\psi(E, z, t) = \sum_{k=-\infty}^{+\infty} \psi_k(z) \exp\left(-\frac{i}{\hbar}(E + k\hbar\Omega)t - i\phi(t) \right) \tag{5.9}$$

with the accumulated phase

$$\phi(t) = \frac{e}{\hbar} \int_0^t dt' \, V_{\mathrm{ac}}(t') = \phi(t + \mathcal{T}) \ . \tag{5.10}$$

Its time-periodicity follows from the zero time-average of the gate voltage. Now the time-dependent Schrödinger equation can be solved by assuming a piecewise constant potential. The heterostructure is cut therefore into layers. At the borders of adjacent layers, the two different wave functions at each side have to be matched. The matching conditions are incorporated into transfer matrices. We presented here only the basic idea of the transfer-matrix technique. A exhaustive overview to this method gives Wagner (1995).

The results discussed here are presented in more depth by Rey, Strass, Kohler, Sols, and Hänggi (2005). Surveying the time-averaged current in Fig. 5.7 calculated numerically from the transfer-matrix method and the Floquet-Green approach within a tight-binding description, we observe current minima for distinct values of $eV_{\mathrm{ac}}/\hbar\Omega$ for frequencies in the microwave regime. The reason for the current suppressions becomes apparent by comparison with the high-frequency approximation along the line of section 5.2, which exhibits minima close to those of the transfer-matrix and tight-binding Floquet-Green curves. The approximate current vanishes whenever the

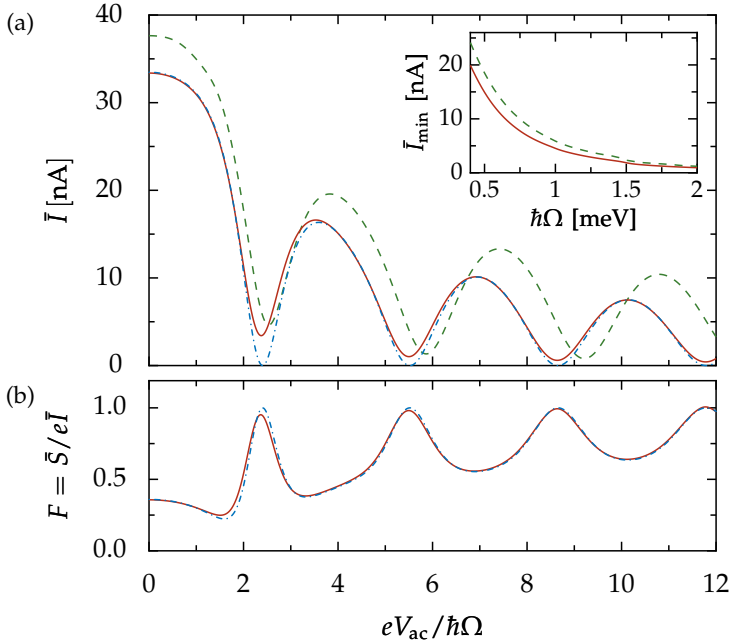

Figure 5.7: (a) Time-average current $\bar{I}$ *vs.* driving amplitude V_{ac} obtained numerically from tight-binding Floquet-Green (solid) and transfer-matrix (dashed line) methods. Also shown is the high-frequency approximation (dashed-dotted). The inset depicts the value of the first current minimum as a function of the driving frequency. Solid (tight-binding) and dashed (transfer-matrix) line decay approximately as $1/\Omega$. (b) Corresponding Fano factor. The chosen parameters are $\hbar\Omega = 1.15\,\text{meV}$, $V = 6.0\,\text{mV}$, $\Gamma = 0.16\,\text{meV}$ and $\Delta = 0.23\,\text{meV}$. The parameters for the barrier structure are those of Fig. 5.6.

ratio $eV_{ac}/\hbar\Omega$ assumes a zero of the Bessel function J_0, *i.e.*, for the values 2.405, 5.520, 8.654, ..., since then $\Delta_{\text{eff}} \propto J_0^2 = 0$. By varying the ratio between driving amplitude and frequency, we can thus tune the tunnelling between the two wells and thereby control the current as already discussed in section 5.2.2. For a frequency $\Omega = 5\Delta/\hbar$, the analytical expression shows a remarkable agreement with the exact Floquet-Green result for $V_{ac} \lesssim V$.

The inset of Fig. 5.7 shows the minimum current at the first suppression decays as a function of the driving frequency Ω. This is expected from the good agreement between the numerical results and the high-frequency approximation, because the approximation accounts for the first order term in a perturbative scheme in $1/\Omega$ [see discussion after Eq. (4.10)]. Higher order contributions are included in a numerically exact calculation, which results in a nonvanishing current at the minima. A similar Ω-dependence is observed also for the transfer-matrix formalism.

While the general shape and magnitude of the current are very similar for both models, there still appears to be a small difference in the location of the minima for the relatively low barriers chosen in Fig. 5.7. For a continuous potential (dashed line), the current assumes minima at values of $eV_{\mathrm{ac}}/\hbar\Omega$ higher than those predicted by the tight-binding description (solid line). We can match the curves even better by using larger barrier heights (Rey, Strass, Kohler, Sols, and Hänggi, 2005). As a consequence, the wave functions of the well states become more localized. This situation corresponds in the tight-binding picture of the Floquet-Green formalism to a lead–well coupling Γ that is almost energy independent and thus mimics the wide-band limit. Furthermore, this argument is used to explain the smaller deviation observed with thinner barriers, since V_{L} is much larger in that case.

The noise strength of the current for the tight-binding approximation described by the Fano factor is depicted in Fig. 5.7(b). For zero driving amplitude, we find $F \approx 1/2$ which is characteristic for the transport through a double barrier as illustrated in Fig. 5.3. Note that the central barrier is considerably lower and, thus, the outer barriers determine the transport. At the current suppression, the central barrier becomes the bottleneck. Then, the setup corresponds to a tunneling point contact with $F \approx 1$. In the crossover region, the transport can be considered "barrier free" and the Fano factor assumes its minimum.

6. Noise in a nonadiabatic electron pump

An alternating potential can induce inelastic tunneling events when the electrons absorb or emit photons from the oscillating external field. If only the exchange of discrete energies is involved, this phenomena is referred to as photon-assisted tunneling (PAT). For an exhaustive review see Platero and Aguado (2004). Quantum dots are especially suited for the experimental implementation of PAT because the discrete dot levels can be readily tuned by means of gate voltages (van der Wiel et al., 2003). In this chapter we explore the case of two coherently coupled quantum dots exposed to microwave radiation in the pumping configuration.

Thereby, in mesoscopic conductors, a cyclic variation of the parameters can induce a pump current: A nonvanishing dc current flows in the absence of any external bias voltage or even against a bias (Kouwenhoven et al., 1991; Pothier et al., 1992; Switkes et al., 1999). If the driving frequency is much larger than the inverse of the typical time-scale for an electron to traverse the conductor, the pump is said to operate in the adiabatic regime (Brouwer, 1998; Altshuler and Glazman, 1999; Moskalets and Büttiker, 2002). For adiabatic quantum pumps, two time-periodic parameters with a phase lag are required. The transfered charge per cycle is determined by the area enclosed in the parameter space during the cyclic evolution (Brouwer, 1998; Altshuler and Glazman, 1999). This implies that the resulting current is proportional to the driving frequency and, thus suggests that in the nonadiabatic regime, electron pumping is more effective. For practical applications, it is not only desirable to yield a large pump current, but also to keep the noise level reasonably low.

It has been found by Avron et al. (2001) that adiabatic pumps can be practically noiseless. This happens, however, at the expense of acquiring a small or even vanishing current (Polianski et al., 2002). Therefore, the question arises whether it is possible to boost the pump current by increasing the driving

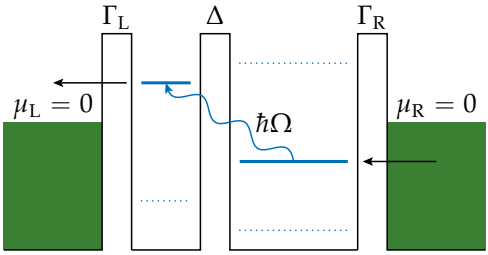

Figure 6.1: Level structure of the asymmetric double quantum dot in a pump configuration ($\mu_L = \mu_R = 0$). The solid lines mark the relevant levels $|1\rangle$ and $|2\rangle$ with the energies $\pm\epsilon_0/2$. The arrows indicate the dominating scattering process of a transmitted electron for the coherent photon-assisted tunneling.

frequency while keeping the noise level very low. Brune et al. (1997) and Stafford and Wingreen (1996) addressed the nonadiabatic pump current in coupled quantum dots theoretically and Oosterkamp et al. (1998) measured it in the regime of strong interdot coupling. However, it was not until recently that the noise characteristics of nonadiabatic quantum pumping has been investigated (Strass et al., 2005a).

6.1. The double-dot model

For reasonable low temperatures (like for helium temperature), intradot excitations do not play a role such that we only consider the lowest unoccupied level in one dot and the highest occupied in the other one. Therefore, each dot is well described by a single energy level as sketched in Fig. 6.1. The double quantum dot Hamiltonian in the discrete level basis of the left and right dot reads

$$\mathcal{H}_{\text{dots}}(t) = -\frac{\Delta}{2}\sigma_x + \frac{\epsilon(t)}{2}\sigma_z \ , \tag{6.1}$$

where the energy difference $\epsilon(t) = \epsilon_0 + A\cos(\Omega t)$ is characterized by the static internal bias ϵ_0 and time-dependent bias stemming form an oscillating gate voltage. Typical driving frequencies range up to 100 GHz (van der Wiel

et al., 1999) such that the wavelength exceeds the size of the setup by far since the extension of double dots is in the sub-micron range. Thus, the implicitly assumed dipole approximation for the driving is well justified. Moreover, the energy scale is set such that $\mu_L = \mu_R = 0$ and therefore the dot levels possess the energies $+\epsilon_0/2$ and $-\epsilon_0/2$, respectively.

6.2. Resonant electron pumping

6.2.1. Symmetry considerations

Before computing the current and the noise, we like to elucidate the symmetries in our system. From classical considerations (Flach et al., 2000), we know that the existence of a dc current in systems driven by time-dependent fields depends on whether symmetry operations are present which lead to a change in the sign of the current, $I(t) \to -I(t)$, and leave the underlying equations of motion invariant. In other words we need some type of symmetry breaking in order to obtain a pump current. This argument applies both for adiabatic and nonadiabatic driving.

For harmonic driving, the total Hamiltonian $H(t)$—including the leads and the tunneling contributions—obeys time-reversal symmetry and hence, each individual scattering process has a time-reversed partner which occurs with the same probability as argued in section 3.2.1. Thus, it is tempting to conclude that the net current of both partners and, consequently, the pump current vanishes in our setup. This, however, is not the case because the driving enables inelastic, *i.e.*, energy nonconserving, scattering. In particular, there exist processes like the one sketched in Fig. 6.1: With the leads initially at equilibrium, an electron from the right lead with energy below the Fermi surface is scattered into a state in the left lead with energy above the Fermi surface. This process contributes to the current. By contrast, the time-reversed process as indicated in 3.1(a) does not transport an electron because the respective initial state is not occupied. The net effect is transport of electrons from the lower level to the higher level, *i.e.*, from right to left.

None the less, the pump might vanish due to the presence of an additional symmetry, such as generalized parity $(x, t) \to (-x, t + \pi/\Omega)$ which relates

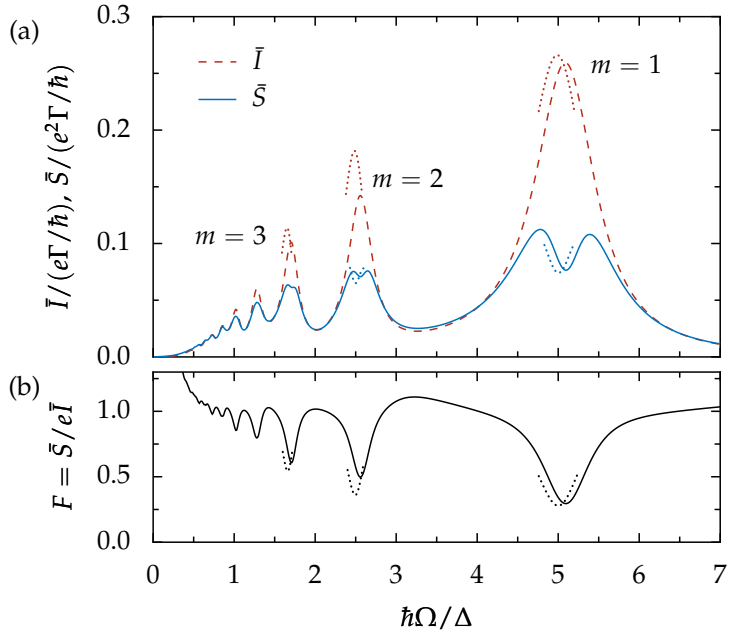

Figure 6.2: (a) Pump current $\bar{I}$ (dashed line) and its noise power $\bar{S}$ (solid) as a function of the driving frequency Ω for coupling strength $\Gamma = 0.3\,\Delta$, driving amplitude $A = 3.7\,\Delta$, and internal bias $\epsilon_0 = 5\,\Delta$. The dotted lines mark the analytical results (6.7) and (6.8) with the first three resonances labeled by their order. Panel (b) depicts the corresponding Fano factor.

two scattering processes with identical *initial* energies as discussed in section 3.2.3. Their contributions to the current cancel each other. With equally strong coupling to the leads, $\Gamma_\mathrm{L} = \Gamma_\mathrm{R} = \Gamma$, generalized parity is satisfied for $H(t)$ solely at zero internal bias $\epsilon_0 = 0$. For finite bias $\epsilon_0 \neq 0$, however, this symmetry is broken and, consequently, a finite pump current emerges. We remark that this current increases proportional to ϵ_0 until the internal bias exceeds the interdot coupling Δ. Moreover, this pump current exhibits resonance peaks depicted in Fig. 6.2 including higher-order resonances as has been already found by Stafford and Wingreen (1996).

6.2.2. High-frequency driving

In order to obtain analytical results within the RWA introduced in chapter 4, we focus on strongly biased situations, $\epsilon_0 \gg \Delta$, and driving frequencies close to the internal resonances of the double dot, $m\hbar\Omega = (\epsilon_0^2 + \Delta^2)^{1/2} \approx \epsilon_0$. In this regime, the dynamics of the dot electrons is dominated by the second term of the Hamiltonian (6.1) while the tunneling contribution, which is proportional to Δ, represents a perturbation. Thus, the time-dependent phase (4.8) becomes

$$\theta_n(t) = \frac{(-1)^n}{2}\left(m\Omega t + \frac{A}{\hbar\Omega}\sin(\Omega t)\right) \ , \tag{6.2}$$

where we used $x_{1/2} = \pm 1/2$ and $r_{1/2} = \pm 1/2$. Note that r_n is not an integer for the chosen setup as a consequence of setting the level energies of the dots to $\pm\epsilon_0/2$. Furthermore, for the effective dot Hamiltonian, we arrive at

$$\mathcal{H}_{\text{dots,eff}} = -\frac{\Delta_{\text{eff}}}{2}\sigma_x - \frac{\delta}{2}\sigma_z \tag{6.3}$$

with $\delta = m\hbar\Omega - \epsilon_0$ and the effective tunnel matrix element

$$\Delta_{\text{eff}} = (-1)^m J_m\left(\frac{A}{\hbar\Omega}\right)\Delta \ , \tag{6.4}$$

where J_m is the mth order Bessel function of the first kind. We remark that the structure of the transformed Hamiltonian (6.3) is similar to the unbiased case [cf. (5.3)] except for the term with the small detuning δ. Accordingly, the impact on the leads is expressed by

$$f_{\text{L/R,eff}}(\epsilon) = \sum_{k=-\infty}^{\infty} J_k^2\left(\frac{A}{2\hbar\Omega}\right) f_{\text{L/R}}\left(\epsilon + \left[k \pm \frac{m}{2}\right]\hbar\Omega\right) \ , \tag{6.5}$$

which can be interpreted as an effective electron occupation number of the levels in lead ℓ. At zero temperature, it exhibits steps at $\epsilon = \mu_\ell + (k \pm m/2)\hbar\Omega$ and is constant elsewhere. Note that in contrast to the energy shift before Eq. (4.19), we shifted here the argument $\epsilon \to \epsilon + (k' \mp m/2)\hbar\Omega$ in order to arrive at symmetric expressions for the left and right electron occupation with respect to zero energy.

Both the dc current and the noise power can be expressed now in terms of the effective transmission probability $T_{\mathrm{eff}}(\epsilon)$ of an electron with energy ϵ. For a two-level system in the wide-band limit, one obtains similar to the derivation in Appendix A

$$T(\epsilon) = \Gamma^2 |G_{12}^{\mathrm{eff}}(\epsilon)|^2 = \frac{\Gamma^2 \Delta_{\mathrm{eff}}^2}{|(2\epsilon - i\Gamma)^2 - \Delta_{\mathrm{eff}}^2 - \delta^2|^2} \ . \tag{6.6}$$

For the remaining evaluation of the energy integrals in the current (4.19) and the noise (4.22), it is important to note that the transmission is practically zero for $\epsilon^2 \gtrsim \Delta_{\mathrm{eff}}^2 + \Gamma^2 + \delta^2$. Thus, for $\hbar\Omega \gtrsim \Delta_{\mathrm{eff}}, \Gamma, \delta$, the effective electron occupation (6.5) is constant in the relevant energy range and can be replaced by its value at $\epsilon = 0$ (cf. Fig. 4.2). This yields close to the mth resonance

$$\bar{I}_{\mathrm{RWA}}^{(m)} = \frac{e\Gamma}{2\hbar} \frac{\lambda_m \Delta_{\mathrm{eff}}^2}{\Delta_{\mathrm{eff}}^2 + \Gamma^2 + \delta^2} \ , \tag{6.7}$$

$$\bar{S}_{\mathrm{RWA}}^{(m)} = \frac{e^2\Gamma}{4\hbar} \frac{\lambda_m^2 \Delta_{\mathrm{eff}}^2 [2(\Gamma^2 + \delta^2)^2 - \Delta_{\mathrm{eff}}^2(\Gamma^2 - 3\delta^2) + \Delta_{\mathrm{eff}}^4]}{(\Delta_{\mathrm{eff}}^2 + \Gamma^2 + \delta^2)^3} + \frac{1 - \lambda_m^2}{2\lambda_m} e I^{(m)} \ , \tag{6.8}$$

where

$$\lambda_m = f_{\mathrm{R,eff}}(0) - f_{\mathrm{L,eff}}(0) = \sum_{|k| \le m/2} J_k^2 \left(\frac{A}{2\hbar\Omega} \right) \tag{6.9}$$

with $|\lambda_m| \le 1$ and k being an integer. Quite remarkably, for resonant driving ($\delta = 0$), the pump current assumes a *maximum* while the noise power $\bar{S}$ generally assumes a local *minimum* as can be seen in Fig. 6.2(a). This results in an even more pronounced minimum for the Fano factor.

6.2.3. Comparison with exact result

Figure 6.2(a) depicts the numerically exact pump current and its noise power at zero temperature. We find that the current exhibits peaks which are located at the resonance frequencies $\Omega = (\epsilon_0^2 + \Delta^2)^{1/2}/m\hbar$ as mentioned earlier. This agrees well with our analytical results (dotted lines), albeit the RWA predicts the location of the current maxima only to zeroth order in Δ, *i.e.*, at

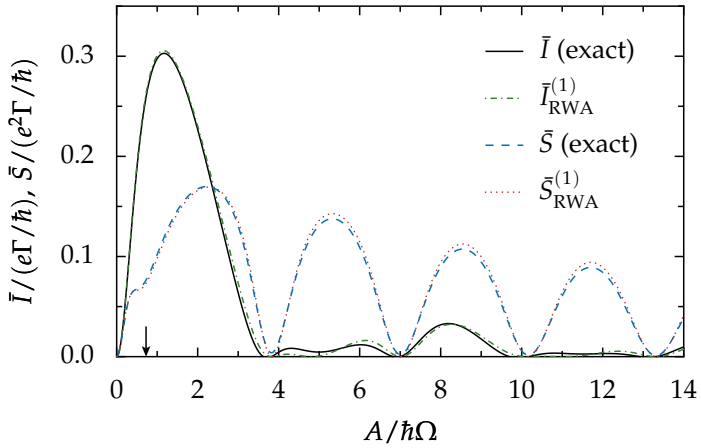

Figure 6.3: Comparison of time-averaged current $\bar{I}$ and zero-frequency noise $\bar{S}$ for exact and approximated result at the first resonance ($m = 1, \delta = 0$) dependent upon the driving amplitude A. The current and noise suppressions coincide with the zeros of $J_1(A/\hbar\Omega)$. The other parameters are as in Fig. 6.2 and the arrow indicates the driving amplitude used in that plot.

the slightly shifted frequencies $\Omega = \epsilon_0/m\hbar$. For the chosen parameters, the zero-frequency noise $\bar{S}$ possesses clear minima, each accompanied by two maxima. In the vicinity of the resonance, the noise is considerably below the shot noise level $e\bar{I}$ looking at Fig. 6.2(b). This feature is notably pronounced at the first resonance. Far from the resonances, the current becomes smaller and the Fano factor is close to $F = 1$.

For the current and noise as a function of the driving amplitude at the first resonance, we find in Fig. 6.3 an excellent agreement between numerical results and the RWA with $\delta = 0$. The reduction of the dc current and the noise strength as a consequence of the coherent suppression of tunneling similar to the unbiased two-level system (cf. Fig. 5.4) is located close to the zeros of the Bessel function J_1 originating from Δ_{eff}. The Bessel function becomes zero for the values $A/\hbar\Omega = 3.812, 7.016, 10.174, \ldots$ Note, however, that the low values for the time-averaged current at every odd noise

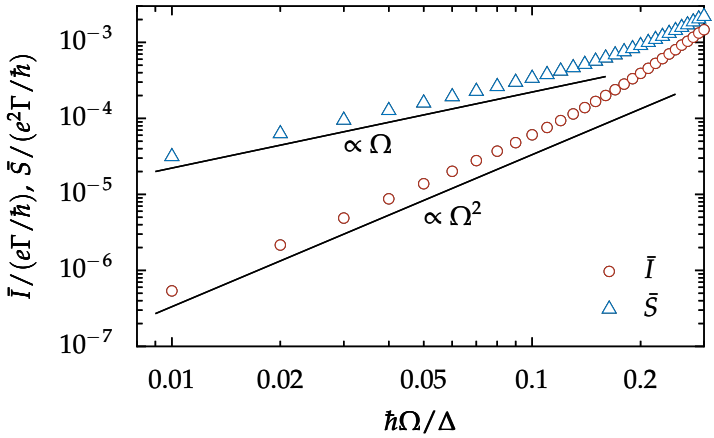

Figure 6.4: Time-averaged current $\bar{I}$ and zero-frequency noise $\bar{S}$ for low driving frequency from Floquet-Green formalism. The plot denotes a blow-up of the lower left corner of Fig. 6.2(a). The straight lines serve as guide to the eyes. The current vanishes as Ω^2 whereas the noise is proportional to Ω.

peak have their origin in the effective electron distributions (6.5) or more correctly speaking in the difference of those which reads $\lambda_1 = J_0^2(A/2\hbar\Omega)$ from the definition (6.9). Furthermore, we observe a characteristic shoulder for $\bar{S}$ (dashed and dotted line) which results in the minimum of the Fano factor depicted in Fig. 6.2 for $m = 1$. The corresponding driving amplitude for this minimum is indicated by the arrow.

6.2.4. Adiabatic *vs.* nonadiabatic pump

As a proof that our Floquet scattering formalism really accounts for the nonadiabatic regime of the electron pump, we consider briefly the adiabatic limit $\Omega \to 0$. Reaching for smaller frequencies, the spectrum of the quasienergies becomes dense and thus also higher sidebands k yield a substantial contribution to the current. Solving the Floquet equation for slow driving is numerically rather costly as a huge number of sidebands have to be considered to assure convergence. Still already Fig. 6.4 clearly reveals that in the

adiabatic limit, the pump current vanishes proportional to Ω^2. This is in contrast to the behavior of electron pumps driven in the adiabatic operational regime as the dc current vanishes linear in Ω there (Moskalets and Büttiker, 2004). For the noise power, however, we observe a linear frequency dependency which is the same as for an adiabatic pump in the low-temperature regime (Moskalets and Büttiker, 2004). Considering the efficiency of nonadiabatic pumping, we find, for instance, for the parameters in Fig. 6.2, that approximately 0.1 electrons are transfered per driving cycle at the first resonance. Ideally, an adiabatic pump can shuffle one electron per cycle across the conductor. However, as the frequency is considerable lower for adiabatic pumping, we obtain a much better efficiency for purely nonadiabatic driving.

6.2.5. Tuning the pump

The comparison of the numerically exact results with the current (6.7) and the noise power (6.8) in Figs. 6.2 and 6.3 leads to the conclusion that the RWA predicts both the current maxima and the noise minima fairly well to employ these expressions for a parameter optimization towards low-noise pumping. We have already seen that the condition of large current and low noise is met at the internal resonances of the biased double-dot setup. Thus, we can restrict the search for optimal parameters to resonant driving with $\hbar\Omega = \epsilon_0/m$. As a figure of merit for the noise strength we employ the Fano factor for $\delta = 0$,

$$F_{\mathrm{RWA}}^{(m)} = \frac{\bar{S}_{\mathrm{RWA}}^{(m)}}{e\bar{I}_{\mathrm{RWA}}^{(m)}} = \frac{1}{2\lambda_m} - \frac{\lambda_m}{2}\frac{\Gamma^2(3\Delta_{\mathrm{eff}}^2 - \Gamma^2)}{(\Delta_{\mathrm{eff}}^2 + \Gamma^2)^2} \quad , \tag{6.10}$$

which is a function of λ_m and $\Delta_{\mathrm{eff}}/\Gamma$. The second term is minimal for $\Delta_{\mathrm{eff}}/\Gamma = \sqrt{5/3}$, yielding $F_{\mathrm{RWA}}^{(m)} = 1/(2\lambda_m) - 9\lambda_m/32$. Thus, the optimal Fano factor is assumed for $\lambda_m = 1$ and reads $F_{\mathrm{opt}} = 7/32 \approx 0.219$. In the following, we restrict ourselves to the fundamental resonance ($m = 1$) for which $\Delta_{\mathrm{eff}} = J_1(A/\hbar\Omega)\Delta$ and $\lambda_1 = J_0^2(A/2\hbar\Omega)$. A similar analysis can be performed also at higher resonances $m > 1$, where the same optimal Fano factor can be reached but for larger driving amplitude. At the first resonance,

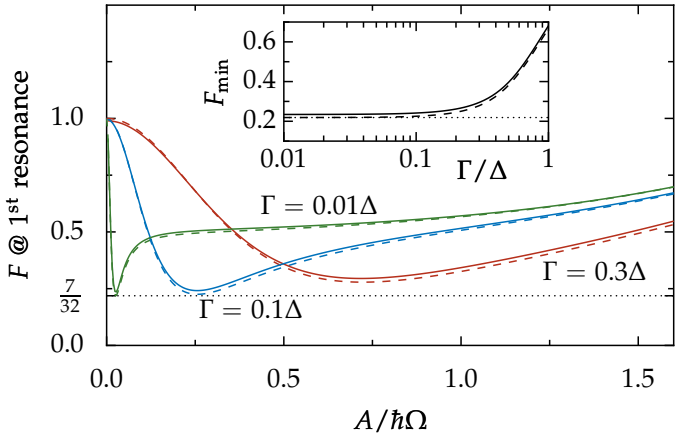

Figure 6.5: Fano factor F at the first resonance ($m = 1$) for various dot–lead coupling strengths Γ. The exact Floquet calculation (solid lines) is compared with the RWA for $\delta = 0$ (dashed). The inset depicts the minimal Fano factor dependent upon Γ for the internal bias $\epsilon_0 = 5\Delta$ at the first resonance. The dotted lines mark the optimal Fano factor $F_{\mathrm{opt}} = 7/32$.

the value $\lambda_1 = 1$ is assumed for $A = 0$ which means $\Delta_{\mathrm{eff}} = 0$; this unfortunately implies a vanishing current (6.7). Therefore, the central question is whether it is possible to find a driving amplitude providing on the one hand an appreciably large pump current, while on the other hand yielding a noise level close to F_{opt}. The numerical results depicted in Fig. 6.5 indeed suggest this possibility: The Fano factor is close to the optimal value already for a finite amplitude. A closer investigation reveals that the location of the minimum corresponds to $\Delta_{\mathrm{eff}} = J_1(A/\hbar\Omega)\Delta = \sqrt{5/3}\,\Gamma$, in compliance with our analytical considerations. In particular, the minimum is shifted towards smaller values of $A/\hbar\Omega$ for weaker coupling Γ. Moreover, we emphasize again that the RWA results (6.7) and (6.8) agree very well with the numerically exact results, although they slightly underestimate the noise.

The data in Fig. 6.5 also reveal that in the interesting regime, the ratio $A/\hbar\Omega$ is considerably smaller than unity and hence, we can employ the approximations $J_0(x) \approx 1 - x^2/4$ and $\mathrm{J}_1(x) \approx x/2$ valid for small arguments.

It is now straightforward to obtain in lowest order of $A/\hbar\Omega$ the expressions $\Delta_{\text{eff}} = A\Delta/2\hbar\Omega$ and $F^{(1)}_{\text{RWA}} = 7/32 + (5A/16\hbar\Omega)^2$.

For instance, choosing $A = 0.3\,\hbar\Omega$, the noise level lies merely 5% above F_{opt} and the condition $\Delta_{\text{eff}} = \sqrt{5/3}\,\Gamma$ corresponds to $\Gamma \approx 0.1\,\Delta$, *i.e.*, to weak dot–lead coupling. This estimate is confirmed by the inset in Fig. 6.5 which, in addition, demonstrates that $F \approx F_{\text{opt}}$ for $\Gamma \lesssim 0.1\,\Delta$. For such a small coupling Γ, interaction-induced electron–electron correlations typically play a minor role.

The typical tunnel coupling Δ between the two dots is characterized by the range of 10–60 μeV (Oosterkamp et al., 1998). Choosing $\Delta = 25\,\mu$eV, the internal bias $\epsilon_0 = 5\,\Delta$ corresponds to the resonance frequency $\Omega = 5\,\Delta/\hbar \approx 2\pi \times 60\,\text{GHz}$. Tuning the lead coupling to $\Gamma = 0.1\,\Delta$ results within the RWA in an optimized pump current of the order 100 pA with a Fano factor $F \approx 0.23$. The relevant measurements for the pump current by Oosterkamp et al. (1998) operate in the strong interdot coupling regime which means that Δ is of the same order as the internal bias ϵ_0. They detected a value of roughly 0.5 pA for the first resonance peak. For this regime, however, the RWA is no longer valid since the required condition $\epsilon_0 \gg \Delta$ is not fulfilled. Unfortunately, it is neither possible to extract from their data the dot–lead coupling Γ which has been used in the experiment. This, and the fact that a very low microwave field power corresponding to the driving amplitude A was presumably applied, render a reliable comparison with the experiment impossible and serve as an explanation for the large discrepancy in terms of the absolute value of the pump current predicted by the RWA.

6.3. Current–voltage characteristics

Finally, exploring the current–voltage (I–V) curve of the asymmetric double dot driven at the first resonance, which is depicted in Fig. 6.6, allows us to gain some specific insight into the discrete energy exchange of the electrons with the external alternating field typical for photon-assisted tunneling. Figure 6.6 also shows the dependency of the noise power on the external bias voltage. So far we operated our setup with zero voltage ($\mu_{\text{L}} = \mu_{\text{R}} = 0$) as

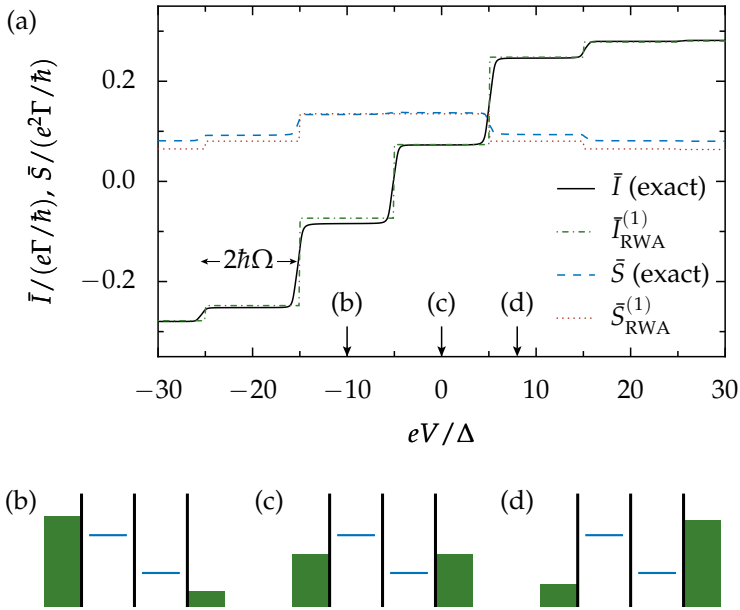

Figure 6.6: (a) Time-averaged current $\bar{I}$ and zero-frequency noise $\bar{S}$ within the exact Floquet-Green formalism and the RWA as a function of the transport voltage V at the 1-photon resonance. The driving amplitude reads $A = 15\,\Delta$ and the remaining parameters are those of Fig. 6.2. The current and its noise strength exhibit steps of width $2\hbar\Omega = 2(\Delta^2 + \epsilon_0^2)^{1/2} = 2\sqrt{26}\,\Delta$ for the chosen parameters and the exact case. The arrows indicate three different transport situations which are illustrated by the energy diagrams in (b), (c) and (d), respectively.

illustrated in Fig. 6.6(c). This *modus operandi* corresponds to the pump configuration. Reaching for higher voltages and approaching the situation of panel (d), a step occurs in the I–V characteristics at $V = (\Delta^2 + \epsilon_0^2)^{1/2}/me$ for the mth resonance.

The enhancement of the current can be comprehended with help of the RWA. For the double dot at resonance ($\delta = 0$), the effective Hamiltonian (6.3) has the same form as in the static case without internal bias ($\epsilon_0 = 0$). The difference in the effective electron distribution (6.5) in presence of a transport

voltage V is modified as

$$\lambda_m = \sum_{|k|\leq K_m(V)} \mathrm{sgn}(V+\epsilon_0)\, J_k^2\left(\frac{A}{2\hbar\Omega}\right) \quad , \tag{6.11}$$

where $K_m(V)$ denotes the largest integer not exceeding $|eV/2\hbar\Omega + m/2|$. Hence, besides the zero photon conduction channel ($k = 0$) for the pump configuration, additional channels also contribute to the current now for the setup in panel (d) since the sum in (6.11) comprises the first sideband $k = -1$ and $k = 1$. Physically, an electron transmitted from the right to the left lead absorbs and emits one photon. The subsequent steps for even higher bias voltage are attributed to larger sideband contributions. The probability for the absorption and the emission processes of k photons is denoted by the square of the Bessel function namely $J_k^2(A/2\hbar\Omega)$.

Going the other way toward negative values of V and approaching the situation in panel (b), the dc current is reversed once the dot levels are aligned with the chemical potentials in the respective lead. Note that based on the fact that a symmetric voltage drop $\mu_\mathrm{L} = -\mu_\mathrm{R}$ is applied in Fig 6.6, the bias voltage is defined as $V = 2\mu_\mathrm{R}/e$. Therefore, also the factor of 2 emerges for the step width of the staircase of the I–V curve which amounts to $2\hbar\Omega$.

Regarding the noise, the conduction channels contribute differently to the noise power. Although the time-averaged current (solid and dashed-dotted lines) is enhanced for positive voltage, the noise power (dashed and dotted lines) exhibits a lower value.

If we decrease the dot–lead coupling as has been done in Fig. 6.7, we observe a sub-structure in the I–V jumps for sufficiently low Γ for the exact Floquet calculation. These intermediate jumps are a consequence of the so-called Rabi splitting (Stafford and Wingreen, 1996). The level in each dot hybridizes with the sidebands of the other level due to the external driving. As the RWA constitutes a degenerate perturbation scheme for the Floquet transport theory, the degeneracy is removed in case of strongly localized states ($\epsilon_0 \gg \Delta$) due to the weak interdot coupling. The corresponding level splitting is obtained by diagonalizing the first order perturbation Hamiltonian defined by (4.10). For the system at hand it corresponds to the effective

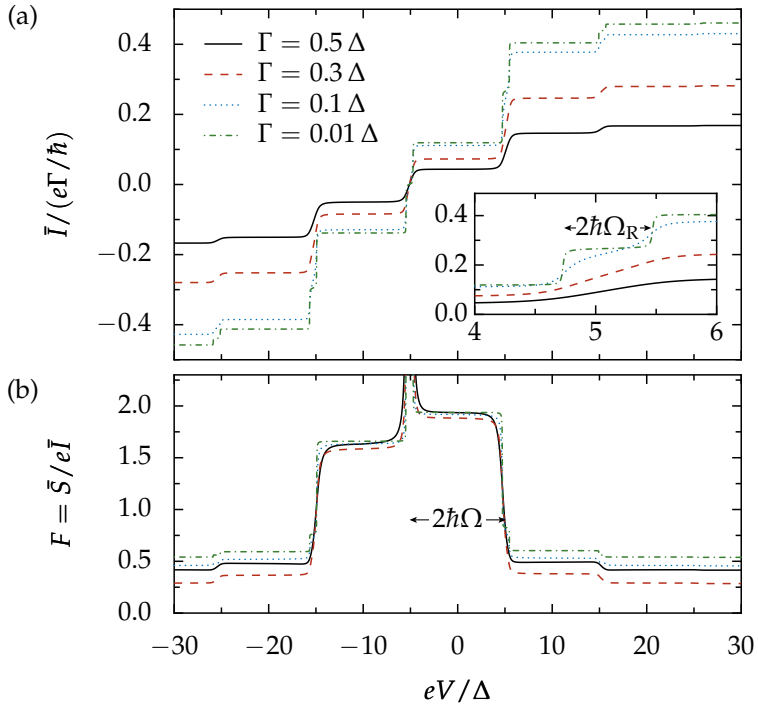

Figure 6.7: Exact calculation of the current–voltage characteristics (a) and the corresponding Fano factor (b) for resonant driving $\Omega = (\Delta^2 + \epsilon_0^2)^{1/2}/\hbar$ and various dot–lead coupling Γ. The driving amplitude is $A = 15\,\Delta$ and the internal bias reads $\epsilon_0 = 5\,\Delta$. The inset reveals an intermediate jump for small coupling strength which is attributed to the Rabi splitting. The step width corresponds to $2\hbar\Omega_R = 2J_1(A/\hbar\Omega)\Delta \approx 0.721\,\Delta$.

Hamiltonian (6.3) and we then obtain for the level splitting

$$\epsilon_\pm = \pm\frac{\Delta}{2}\,J_m\left(\frac{A}{\hbar\Omega}\right) \tag{6.12}$$

at the mth photon resonance. The corresponding Rabi frequency thus reads

$$\Omega_R = \frac{|\epsilon_+ - \epsilon_-|}{\hbar} = \frac{\Delta}{\hbar}\,J_m\left(\frac{A}{\hbar\Omega}\right) \quad . \tag{6.13}$$

The dot–lead coupling has to be sufficiently low in order to resolve the small Rabi splitting since for zero temperature the width of the jumps is determined solely by the coupling constant Γ. Hence, the condition $\Gamma \ll \Omega_R$ must hold. Similar to the step width of the big steps, the factor of 2 in the step width of the intermediate jumps $2\hbar\Omega_R$ is a result of the symmetric voltage drop.

7. Summary and outlook

In this thesis, we studied in a Floquet-Green formalism the noise characteristics of nanoscale conductors under the influence of an oscillating external field. In the first part we derived general expressions for the time-averaged current and the zero-frequency noise in terms of the retarded Green function by solving the Heisenberg equations of motion. Thereby, the metallic leads are eliminated in favor of a self-energy term. The form of the dc current implies transmission probabilities which incorporate inelastic scattering channels. Hence, our approach can be interpreted as an extension of the Landauer formalism to time-dependent scattering. As a next step, we presented an expansion of the retarded Green function in terms of a Floquet ansatz for which the electrons are effectively noninteracting in order to obtain an efficient, numerically exact solution.

Developing a perturbation scheme based on Floquet theory, the driven system has been reduced to an effectively time-independent problem with a renormalized wire Hamiltonian and renormalized electron distributions. This scheme is applicable for high-frequency driving which is relevant for many experiments. In particular, it also works for the resonant case, as long as the photon energy of the driving field defines the largest energy scale of the system. Hence, this perturbative solution of the time-dependent problem can be interpreted as a rotating wave approximation for driven transport. It allows one to evaluate *analytically* the transport properties with the help of the current and the noise expressions for the static case, but with the renormalized quantities mentioned above.

This approach proves to be extremely successful in order to elucidate the mechanism for the shot noise suppressions that we observe for an unbiased two-level system. The results of the high-frequency approximation are indeed in excellent agreement with the numerically exact outcome from the Floquet scattering formalism. We find that the purely coherent influence

of an oscillating external field can suppress transport in the manner of the coherent destruction of tunneling. Depending on the ratio of driving amplitude and driving frequency, the time-averaged current and the noise power assume characteristic minima. The relative noise strength characterized by the Fano factor exhibits remarkably low minimal values in the vicinity of current suppressions.

Consequently, the results of this work demonstrate that the control of a current through a molecule by means of a time-periodic driving provides a viable alternative to the traditional single electron transistor setup based on a gate electrode. Furthermore, a suitable choice of the transistor's working point permits operation in a low noise regime with a small Fano factor. The current and noise properties that we found for the driven quantum system hopefully prove to be useful for the development of novel molecular electronics devices. In any case, they yield a qualitative understanding of the underlying transport mechanism.

As a further result, we showed that our driven tight-binding model can be matched with a transfer-matrix approach which is a standard technique to compute the exact tunneling currents in heterostructures. For the setup of a triple-barrier structure driven by an alternating gate voltage, we compared the dc current obtained within the two methods. Again, we verified the effect of coherent suppression of tunneling. By adjusting the barrier heights, we came to the conclusion that the two different approaches yield very similar results under the condition that the barriers are sufficiently high. Large barrier heights assure energy-independent coupling constants which are inherent to our model system. Hence, the Floquet scattering formalism together with the analytical approximation provides a valid tool for studying theoretically the coherent control of time-dependent electron transport which can be investigated with today's semiconductor technology.

Exploring coherently coupled quantum dots, we moreover discussed the intriguing phenomena of nonadiabatic electron pumping. As a consequence of the spatial asymmetry of the double dot, the ac driven setup provides a dc current although no external bias voltage has been applied. Effective electron pumping is accomplished for resonant driving beyond the adiabatic regime. With the help of the rotating wave approximation we obtained

an analytical solution for the transport problem, which allowed us to determine systematically the ideal *modus operandi*. We conclude that a large internal bias at resonant driving in combination with a weak dot–lead coupling is required. In particular, the pump current assumes a maximum while the (absolute) noise power exhibits at the same time a minimum. Hence, the resulting minimum for the Fano factor is even more pronounced. Our finding convincingly suggests that coupled quantum dots are ideal for pumping electrons effectively and reliably at a low noise level.

Considering a molecular setup, the stability of metal–molecule–metal junctions is still a major issue. To the best of the author's knowledge, no conduction measurements for molecules irradiated by laser light have been conducted successfully so far, although currently attempted by several groups. Within the standard method of open break-junctions, the pointed illumination of molecules denotes a truly challenging task because thermal effects stemming from the irradiation of the leads are dominant. However, a very promising approach might be the implementation of near-field T-tips (Matzelle et al., 2003; Fischer, 1993). Here, a cutting edge of a glass substrate is coated with a metallic film on the touching sides such that the edge itself remains uncoated. When bringing this tip close to an opposite metal substrate, the molecules can bridge the gap by chemisorption to the metal surfaces. Now shining with a laser onto the glass, the tip acts as a prism focusing the light on the molecule without illuminating the leads.

The measurement of shot noise properties in driven nanoconductors is a rather delicate subject. To measure shot noise in molecular systems seems to as a consequence of the stability issues discussed in the previous paragraph a highly nontrivial task. However, for heterostructures at sufficiently low temperatures—in order to suppress the background of $1/f$-noise—the situation is much more promising. Very recent experiments by Song et al. measuring photo-generated electron tunneling through multiple barriers in an undoped superlattice structure indicated that the Fano factor approaches values close to $1/3$ for weak driving, *i.e.*, in the low-electric field regime.

In the context of driven transport, there are more questions that deserve a future investigation. A fascinating field is the heat transport in nanoscale conductors connected to leads. The energy transfer in such systems can be

evaluated within the framework of our Floquet-Green formalism. An interesting question is, for instance, whether it is possible to extract heat from one of the leads depending on the driving of the external field. As a further extension of our model it would be desirable to explore the role of electron–electron interactions for time-dependent systems. However, the Floquet scattering approach presented here can not be generalized for this case straightforwardly. For this purpose, a many-particle Floquet theory has to be developed which is a very demanding task.

A. Static conductor

In order to interpret the results for the current and the noise for driven quantum wires, it is very helpful to consider the time-independent case. The Landauer scattering formula for the current has already been introduced in 2.2.1. To check our time-dependent scattering approach for consistency, we will verify that in the static limit the current and the noise power derived in chapter 2 match the established results known in literature. In addition, we derive analytical expression for a two-level and a three-level system in the limit of a large voltage drop and energy-independent lead–wire coupling.

A.1. Scattering formalism

By setting the driving amplitude $A = 0$ in the wire Hamiltonian (3.1), the time-reversal symmetry is contained. Since no inelastic scattering channels are present in the time-independent system, all sidebands except for $k = 0$ disappear. This leads to $T^{(0)}_{\mathrm{LR}}(E) = T^{(0)}_{\mathrm{RL}}(E) = T(E)$ according to Eq. (3.36). The transmission probability of electrons transmitted across the wire thus reads

$$T(E) = \Gamma_{\mathrm{L}}(E)\Gamma_{\mathrm{R}}(E)|G_{1N}(E)|^2 \tag{A.1}$$

with the retarded Green function of the static situation calculated via

$$G(E) = [E\mathbb{1} - \mathcal{H}_{\mathrm{wire}} - i\Sigma]^{-1} \ . \tag{A.2}$$

Note that the spectral density is assumed to be energy dependent. Therefore, no wide-band limit is applied here. Inserting the transmission function into the formula (2.36), the current assumes the same form as for the Landauer approach which is—for the sake of completeness—stated once more

$$I = \frac{e}{h}\int dE\, T(E)\,[f_{\mathrm{R}}(E) - f_{\mathrm{L}}(E)] \ . \tag{A.3}$$

This formula or variations thereof has been derived for sundry mesoscopic structures within the framework of linear-response theory (Langreth and Abrahams, 1981; Engquist and Anderson, 1981; Sols, 1991) and nonequilibrium Green function techniques (Wingreen et al., 1993; Wacker and Jauho, 1998)—just to name a few. To compute the zero-frequency noise of a static conductor, it is convenient to employ the relation

$$|\Gamma_{\mathrm{L}} G_{11}(E) + i|^2 = 1 - T(E) \tag{A.4}$$

noted by Datta (1995) in order to eliminate the back-scattering terms in the noise formula (2.40). By doing so, the current noise does not depend on the phase of the transmission amplitude in contrast to the time-dependent case. Finally, we arrive at the result

$$\begin{aligned} S = \frac{e^2}{h} \int dE \Big\{ & T(E)[f_{\mathrm{L}}(E)\bar{f}_{\mathrm{L}}(E) + f_{\mathrm{R}}(E)\bar{f}_{\mathrm{R}}(E)] \\ & + T(E)[1 - T(E)][f_{\mathrm{R}}(E) - f_{\mathrm{L}}(E)]^2 \Big\} \ , \end{aligned} \tag{A.5}$$

which matches exactly the expression already obtained by Büttiker (1992). Again the shorthand notation $\bar{f}_\ell(E) = 1 - f_\ell(E)$ has been adopted. Two different contributions are characterized by the zero-frequency noise in the static limit as remarked by Blanter and Büttiker (2000). The terms in the first line describe the temperature-dependent equilibrium quantum noise also called Johnson-Nyquist noise according to the dissipation-fluctuation theorem (Callen and Welton, 1951). It vanishes for zero temperature and for a finite bias voltage $V \neq 0$, only the shot noise in the second line is present then. It is easily verified that if both temperature and bias voltage are zero, the current, as well as the noise, vanish. It should not pass uncommented that in presence of a driving field, *i.e.*, $A \neq 0$, this is no longer the case.

A.2. Two-level system

To explicitly exemplify the derivation for the current and the noise power, a two-level system with no internal bias is considered. The derivation mimics

Kohler, Camalet, Strass, Lehmann, Ingold, and Hänggi (2004). For convenience, the energy scale is chosen such that the on-site energy of the two resonant levels are zero and are situated exactly halfway between the transport bias window defined by the chemical potentials μ_R and μ_L (see Fig. 5.1). In the wide-band limit (2.8), the Heisenberg equations of motion read

$$\dot{c}_1 = \frac{i}{\hbar}\Delta c_2 - \frac{\Gamma_L}{2\hbar}c_1 + \xi_L(t) \ , \tag{A.6}$$

$$\dot{c}_2 = \frac{i}{\hbar}\Delta c_1 - \frac{\Gamma_R}{2\hbar}c_2 + \xi_R(t) \ . \tag{A.7}$$

The solution of these two inhomogeneous equations in the asymptotic limit $t_0 \to -\infty$ yields

$$c_n(t) = \int_0^\infty d\tau \left[G_{n1}(\tau)\xi_L(t-\tau) + G_{n2}(\tau)\xi_R(t-\tau)\right] \tag{A.8}$$

with $n = 1, 2$. Assuming equal coupling to the leads, $\Gamma_L = \Gamma_R = \Gamma$, the retarded Green function is given by

$$G(\tau) = e^{-\Gamma\tau/2\hbar}\begin{pmatrix} \cos(\Delta\tau/\hbar) & i\sin(\Delta\tau/\hbar) \\ i\sin(\Delta\tau/\hbar) & \cos(\Delta\tau/\hbar) \end{pmatrix}\Theta(\tau) \ , \tag{A.9}$$

where $\Theta(\tau)$ is the Heaviside function. $G(\tau)$ depends solely on the time difference contrary to the driven case. According to Eq. (A.1), the transmission becomes

$$T(E) = \frac{\Gamma^2\Delta^2}{|(E - i\Gamma/2)^2 - \Delta^2|^2} \ . \tag{A.10}$$

We now consider voltages larger than all other energy scales in the problem. As a consequence, the current noise will entirely be due to shot noise. In the expression (A.3) for the current, the difference of the Fermi distributions practically equals one for energies where the transmission is nonvanishing in the limit of large voltages. Then, the results for the current and the noise strength will not depend on temperature. The current thus reads

$$I_\infty = \frac{e}{2\pi\hbar}T = \frac{e\Gamma}{2\hbar}\frac{\Delta^2}{\Delta^2 + (\Gamma/2)^2} \ , \tag{A.11}$$

where $T = \int dE\, T(E)$ is the total transmission. With the same line of reasoning we find from Eq. (A.5) for the zero-frequency noise

$$S_\infty = \frac{e^2\Gamma}{\hbar}\frac{2\Delta^2(\Gamma^4 - 2\Gamma^2\Delta^2 + 8\Delta^4)}{(4\Delta^2+\Gamma^2)^3} \quad . \tag{A.12}$$

The Fano factor $F = S/eI$ becomes

$$F_\infty = \frac{\Gamma^4 - 2\Gamma^2\Delta^2 + 8\Delta^4}{(4\Delta^2+\Gamma^2)^2} \quad . \tag{A.13}$$

This relative noise level reaches its minimum at $\Delta = \sqrt{5/12}\Gamma$ which means the transport across the two-level system is optimal there.

A.3. Three-level system

Similar for a three-level system, the quantities characterizing transport can be calculated analytically (Strass et al., 2005b). The on-site energies are again set to zero. For the transmission, one obtains

$$T(E) = \frac{\Gamma^2\Delta^2}{|(2iE+\Gamma)(2iE^2+E\Gamma-4i\Delta^2)|^2}. \tag{A.14}$$

For the current, the expression (A.11) as for the two-level system is acquired. However, the noise results in

$$S_\infty = \frac{e^2\Gamma}{\hbar}\frac{\Delta^2(\Gamma^4 - 4\Gamma^2\Delta^2 + 16\Delta^4)}{(4\Delta^2+\Gamma^2)^3} \tag{A.15}$$

and the corresponding Fano factor reads

$$F_\infty = \frac{\Gamma^4 - 4\Gamma^2\Delta^2 + 16\Delta^4}{2(4\Delta^2+\Gamma^2)^2} \quad . \tag{A.16}$$

The minimal Fano factor $F_\infty = 1/8$ is obtained for $\Delta = \Gamma/2$.

References

N. Agraït, A. L. Yeyati, and J. M. van Ruitenbeek, *Quantum properties of atomic-sized conductors*, Phys. Rep. **377**, 81 (2003). (cited on page 2)

L. Allen and J. H. Eberly, *Optical Resonances and Two-Level Atoms* (Wiley, New York, 1975). (cited on page 45)

B. L. Altshuler and L. I. Glazman, *Pumping Electrons*, Science **283**, 1864 (1999). (cited on page 59)

P. K. Aravind and J. O. Hirschfelder, *Two-state systems in semiclassical and quantized fields*, J. Phys. Chem. **88**, 4788 (1984). (cited on page 23)

L. Arrachea, *Green-function approach to transport phenomena in quantum pumps*, Phys. Rev. B **72**, 125349 (2005). (cited on page 25)

N. W. Ashcroft and N. D. Mermin, *Solid State Physics* (Saunders College Publishing, Fort Worth, 1976). (cited on page 26)

D. Astumian and P. Hänggi, *Brownian motors*, Phys. Today **55** (11), 33 (2002). (cited on page 4)

A. Aviram and M. A. Ratner, *Molecular Rectifiers*, Chem. Phys. Lett. **29**, 277 (1974). (cited on page 1)

J. E. Avron, A. Elgart, G. M. Graf, and L. Sadun, *Optimal Quantum Pumps*, Phys. Rev. Lett. **87**, 236601 (2001). (cited on page 59)

C. Beenakker and C. Schönenberger, *Quantum Shot Noise*, Phys. Today **56** (11), 37 (2003). (cited on page 2)

C. W. J. Beenakker and H. van Houten, *Quantum transport in semiconductor nanostructures*, Solid State Phys. **44**, 1 (1991). (cited on page 54)

Y. M. Blanter and M. Büttiker, *Shot noise in mesoscopic conductors*, Phys. Rep. **336**, 1 (2000). (cited on pages 2 and 80)

R. H. Blick, R. J. Haug, J. Weis, D. Pfannkuche, K. von Klitzing, and K. Eberl, *Single-electron tunneling through a double quantum dot: The artificial molecule*, Phys. Rev. B **53**, 7899 (1996). (cited on page 3)

P. W. Brouwer, *Scattering approach to parametric pumping*, Phys. Rev. B **58**, R10135 (1998). (cited on page 59)

P. Brune, C. Bruder, and H. Schoeller, *Photon-assisted transport through ultrasmall quantum dots: Influence of intradot transitions*, Phys. Rev. B **56**, 4730 (1997). (cited on pages 4 and 60)

M. Büttiker, *Scattering theory of current and intensity noise correlations in conductors and wave guides*, Phys. Rev. B **46**, 12485 (1992). (cited on page 80)

H. B. Callen and T. A. Welton, *Irreversibility and Generalized Noise*, Phys. Rev. **83**, 34 (1951). (cited on page 80)

S. Camalet, S. Kohler, and P. Hänggi, *Shot-noise control in ac-driven nanoscale conductors*, Phys. Rev. B **70**, 155326 (2004). (cited on pages 7, 10, and 45)

S. Camalet, J. Lehmann, S. Kohler, and P. Hänggi, *Current noise in ac-driven nanoscale conductors*, Phys. Rev. Lett. **90**, 210602 (2003). (cited on pages 7, 45, and 51)

F. Capasso and S. Datta, *Quantum Electron Devices*, Phys. Today **43** (2), 74 (1990). (cited on page 54)

C. Caroli, R. Combescot, P. Nozieres, and D. Saint-James, *Direct calculation of the tunneling current*, J. Phys. C **4**, 916 (1971). (cited on page 12)

L. Y. Chen and C. S. Ting, *Theoretical investigation of noise characteristics of double-barrier resonant-tunneling systems*, Phys. Rev. B **43**, 4534 (1991). (cited on page 51)

C. Cohen-Tannoudji, J. Dupont-Roc, and G. Grynberg, *Atom-Photon Interaction: Basic Processes and Applications* (John Wiley & Sons, New York, 1992). (cited on page 31)

C. E. Creffield and G. Platero, *ac-driven localization in a two-electron quantum dot molecule*, Phys. Rev. B **65**, 113304 (2002). (cited on page 45)

G. Cuniberti, G. Fagas, and K. Richter (eds.), *Introducing Molecular Electronics*, vol. 680 of *Lecture Notes in Physics* (Springer, Berlin Heidelberg, 2005). (cited on page 2)

P. Curie, *Sur la symétrie dans les phénomenes physiques, symétrie d'un champ électrique et d'un champ magnétique*, J. Phys. (Paris) 3. Série (théorique et appliqué) **3**, 393 (1894). (cited on page 31)

S. Datta, *Electronic Transport in Mesoscopic Systems*, vol. 3 of *Cambridge Studies in Semiconductor Physics and Microelectronic Engineering* (Cambridge University Press, Cambridge, 1995). (cited on pages 4, 16, and 80)

S. Datta and M. P. Anantram, *Steady-state transport in mesoscopic systems illuminated by alternating fields*, Phys. Rev. B **45**, 13761 (1992). (cited on pages 4 and 17)

R. de Picciotto, M. Reznikov, M. Heiblum, V. Umansky, G. Bunin, and D. Mahalu, *Direct observation of a fractional charge*, Nature **389**, 162 (1997). (cited on page 21)

H.-L. Engquist and P. W. Anderson, *Definition and measurement of the electrical and thermal resistances*, Phys. Rev. B **24**, 1151 (1981). (cited on page 80)

L. Esaki and R. Tsu, *Superlattice and Negative Differential Conductivity in Semiconductors*, IBM J. Res. Dev. **14**, 61 (1970). (cited on page 54)

U. Fano, *Ionization Yield of Radiations. II. The Fluctuations of the Number of Ions*, Phys. Rev. **72**, 26 (1947). (cited on page 21)

R. P. Feynman, R. B. Leighton, and M. Sands, *The Feynman Lectures on Physics*, vol. 1 (Addison Wesley, Reading MA, 1963). (cited on page 4)

U. C. Fischer, in: *Near field optics*, edited by D. W. Pohl (Kluwer, Dordrecht, 1993), vol. 242 of *Nato ASI series E*. (cited on page 77)

D. S. Fisher and P. A. Lee, *Relation between conductivity and transmission matrix*, Phys. Rev. B **23**, 6851 (1981). (cited on pages 12 and 19)

S. Flach, O. Yevtushenko, and Y. Zolotaryuk, *Directed Current due to Broken Time-Space Symmetry*, Phys. Rev. Lett. **84**, 2358 (2000). (cited on pages 30 and 61)

G. Floquet, *Sur les équations différentielles linéaires à coefficients périodiques*, Ann. de l'Ecole Norm. Sup. **12**, 47 (1883). (cited on page 25)

N. J. Geddes, J. R. Sambles, D. J. Jarvis, W. G. Parker, and D. J. Sandman, *The Electrical-Properties of Metal-Sandwiched Langmuir-Blodgett Multilayers and Monolayers of a Redox-Active Organic Molecular-Compound*, J. Appl. Phys. **71**, 756 (1992). (cited on page 1)

H. Grabert, U. Weiss, and P. Talkner, *Quantum-theory of the damped harmonic-oscillator*, Z. Phys. B **55**, 87 (1984). (cited on page 14)

M. Grifoni and P. Hänggi, *Driven Quantum Tunneling*, Phys. Rep. **304**, 229 (1998). (cited on pages 15, 23, and 29)

F. Grossmann, T. Dittrich, P. Jung, and P. Hänggi, *Coherent Destruction of Tunneling*, Phys. Rev. Lett. **67**, 516 (1991). (cited on pages 5, 37, and 45)

F. Grossmann and P. Hänggi, *Localization in a Driven Two-Level Dynamics*, Europhys. Lett. **18**, 571 (1992). (cited on pages 37 and 39)

F. Grossmann, P. Jung, T. Dittrich, and P. Hänggi, *Tunneling in a periodically driven bistable system*, Z. Phys. B **84**, 315 (1991). (cited on page 36)

P. Hänggi, S. Kohler, J. Lehmann, and M. Strass, *AC-driven transport through molecular wires*, in: *Introducing Molecular Electronics*, edited by G. Cuniberti, G. Fagas, and K. Richter (Springer, Berlin Heidelberg, 2005), vol. 680 of *Lecture Notes in Physics*, pp. 55–75. (cited on page 7)

P. Hänggi, M. Ratner, and S. Yaliraki (eds.), *Special Issue: Processes in Molecular Wires*, vol. 281 of *Chemical Physics* (Elsevier, Amsterdam, 2002). (cited on page 2)

J. R. Heath and M. A. Ratner, *Molecular Electronics*, Phys. Today **56** (11), 43 (2003). (cited on page 2)

M. Holthaus, *Collapse of minibands in far-infrared irradiated superlattices*, Phys. Rev. Lett. **69**, 351 (1992a). (cited on pages 37 and 45)

M. Holthaus, *The quantum-theory of an ideal superlattice responding to far-infrared laser-radiation*, Z. Phys. B **89**, 251 (1992b). (cited on page 36)

Y. Imry, *Introduction to Mesoscopic Physics*, vol. 1 of *Mesoscopic Physics and Nanotechnology* (Oxford University Press, New York, 1997). (cited on pages 4 and 54)

Y. Imry and R. Landauer, *Conductance viewed as transmission*, Rev. Mod. Phys. **71**, S306 (1999). (cited on page 4)

A.-P. Jauho, N. S. Wingreen, and Y. Meir, *Time-dependent transport in interacting and noninteracting resonant-tunneling systems*, Phys. Rev. B **50**, 5528 (1994). (cited on pages 4 and 12)

C. Joachim, J. K. Gimzewski, and A. Aviram, *Electronics using hybrid-molecular and mono-layer devices*, Nature **408**, 541 (2000). (cited on page 2)

F. Jülicher, A. Adjari, and J. Prost, *Modeling Molecular Motors*, Rev. Mod. Phys. **69**, 1269 (1997). (cited on page 4)

M. A. Kastner, *Artificial Atoms*, Phys. Today **46** (1), 24 (1993). (cited on page 3)

S. Kohler, S. Camalet, M. Strass, J. Lehmann, G.-L. Ingold, and P. Hänggi, *Charge transport through a molecule driven by a high-frequency field*, Chem. Phys. **296**, 243 (2004). (cited on pages 37, 45, and 81)

S. Kohler, J. Lehmann, and P. Hänggi, *Driven quantum transport on the nanoscale*, Phys. Rep. **406**, 379 (2005). (cited on pages 2 and 7)

L. P. Kouwenhoven, A. T. Johnson, N. C. van der Vaart, C. J. P. M. Harmans, and C. T. Foxon, *Quantized current in a quantum-dot turnstile using oscillating tunnel barriers*, Phys. Rev. Lett. **67**, 1626 (1991). (cited on page 59)

R. Landauer, *Spatial Variation of Currents and Fields Due to Localized Scatterers in Metallic Conduction*, IBM J. Res. Dev. **1**, 223 (1957). (cited on pages 4 and 11)

R. Landauer, *Electrical resistance of disordered one-dimensional lattices*, Philos. Mag. **21**, 863 (1970). (cited on page 11)

R. Landauer, *Conductance from Transmission – Common-Sense Points*, Phys. Scripta **T42**, 110 (1992). (cited on page 4)

D. C. Langreth and E. Abrahams, *Derivation of the Landauer conductance formula*, Phys. Rev. B **24**, 2978 (1981). (cited on page 80)

R. B. Laughlin, *Anomalous Quantum Hall Effect - An Incompressible Quantum Fluid with Fractionally Charged Excitations*, Phys. Rev. Lett. **50**, 1395 (1983). (cited on page 21)

J.-O. Lee, G. Lientschnig, F. Wiertz, M. Struijk, R. A. J. Janssen, R. Egberink, D. N. Reinhoudt, P. Hadley, and C. Dekker, *Absence of Strong Gate Effects in Electrical Measurements on Phenylene-Based Conjugated Molecules*, Nano Lett. **3**, 113 (2003). (cited on page 3)

J. Lehmann, S. Camalet, S. Kohler, and P. Hänggi, *Laser controlled molecular switches and transistors*, Chem. Phys. Lett. **368**, 282 (2003a). (cited on pages 3, 45, and 47)

J. Lehmann, S. Kohler, P. Hänggi, and A. Nitzan, *Rectification of laser-induced electronic transport through molecules*, J. Chem. Phys. **118**, 3283 (2003b). (cited on pages 30 and 35)

Y. Levinson, O. Entin-Wohlman, and P. Wölfle, *Acoustoelectric Current and Pumping in a Ballistic Point Contact*, Phys. Rev. Lett. **85**, 634 (2000). (cited on page 3)

W. Liang, M. P. Shores, M. Bockrath, J. R. Long, and H. Park, *Kondo resonance in a single-molecule transistor*, Nature **417**, 725 (2002). (cited on page 3)

H. Linke, T. E. Humphrey, A. Löfgren, A. O. Shuskov, R. Newbury, R. P. Taylor, and P. Omling, *Experimental tunneling ratchets*, Science **286**, 2314 (1999). (cited on page 30)

N. L. Manakov, V. D. Ovsiannikov, and L. P. Rapoport, *Atoms in a laser field*, Phys. Rep. **141**, 319 (1986). (cited on page 23)

B. Mann and H. Kuhn, *Tunneling through fatty acid salt monolayers*, J. Appl. Phys. **42**, 4398 (1971). (cited on page 1)

D. F. Martinez, *Floquet-Green function formalism for harmonically driven Hamiltonians*, J. Phys. A-Math. Gen. **36**, 9827 (2003). (cited on page 25)

D. F. Martinez, *High-order harmonic generation and dynamic localization in a driven two-level system, a non-perturbative solution using the Floquet-Green formalism*, J. Phys. A-Math. Gen. **38**, 9979 (2005). (cited on page 25)

T. R. Matzelle, H. Gnaegi, A. Ricker, and R. Reichelt, *Characterization of the cutting edge of glass and diamond knives for ultramicrotomy by scanning force microscopy using cantilevers with a defined tip geometry. Part II*, J. Microsc.-Oxford **209**, 113 (2003). (cited on page 77)

Y. Meir and N. S. Wingreen, *Landauer formula for the current through an interacting electron region*, Phys. Rev. Lett. **68**, 2512 (1992). (cited on pages 12 and 14)

R. M. Metzger, *Unimolecular electrical rectifiers*, Chem. Rev. **103**, 3803 (2003). (cited on page 1)

R. M. Metzger, B. Chen, U. Hopfner, M. V. Lakshmikantham, D. Vuillaume, T. Kawai, X. L. Wu, H. Tachibana, T. V. Hughes, H. Sakurai, et al., *Unimolecular electrical rectification in hexadecylquinolinium tricyanoquinodimethanide*, J. Am. Chem. Soc. **119**, 10455 (1997). (cited on page 1)

P. M. Morse and H. Freshbach, *Methods of Theoretical Physics – Part I* (McGraw-Hill, New York, 1953). (cited on pages 28 and 30)

M. Moskalets and M. Büttiker, *Floquet scattering theory of quantum pumps*, Phys. Rev. B **66**, 205320 (2002). (cited on page 59)

M. Moskalets and M. Büttiker, *Floquet scattering theory for current and heat noise in large amplitude adiabatic pumps*, Phys. Rev. B **70**, 245305 (2004). (cited on page 67)

S. G. Narendra and A. Chandrakasan (eds.), *Leakage in Nanometer CMOS Technologies*, Series on Integrated Circuits and Systems (Springer, Berlin Heidelber, 2005). (cited on page 1)

A. Nitzan, M. Galperin, G.-L. Ingold, and H. Grabert, *On the electrostatic potential profile in biased molecular wires*, J. Chem. Phys. **117**, 10837 (2002). (cited on page 46)

A. Nitzan and M. A. Ratner, *Electron transport in molecular wire junctions*, Science **300**, 1384 (2003). (cited on page 2)

T. H. Oosterkamp, T. Fujisawa, W. G. van der Wiel, K. Ishibashi, R. V. Hijman, S. Tarucha, and L. P. Kouwenhoven, *Microwave spectroscopy of a quantum-dot molecule*, Nature **395**, 873 (1998). (cited on pages 4, 60, and 69)

B. Pellegrini, *Extension of the electrokinematics theorem to the electromagnetic-field and quantum-mechanics*, Il Nuovo Cimento **15**, 855 (1993). (cited on page 24)

G. Platero and R. Aguado, *Photon-assisted transport in semiconductor nanostructures*, Phys. Rep. **395**, 1 (2004). (cited on page 59)

S. Pleutin, H. Grabert, G.-L. Ingold, and A. Nitzan, *The electrostatic potential profile along a biased molecular wire: A model quantum-mechanical calculation*, J. Chem. Phys. **118**, 3756 (2003). (cited on page 46)

M. L. Polianski, M. G. Vavilov, and P. W. Brouwer, *Noise through quantum pumps*, Phys. Rev. B **65**, 245314 (2002). (cited on page 59)

H. Pothier, P. Lafarge, C. Urbina, D. Esteve, and M. H. Devoret, *Single-electron pump based on charging effects*, Europhys. Lett. **17**, 249 (1992). (cited on page 59)

I. I. Rabi, N. F. Ramsey, and J. Schwinger, *Use of Rotating Coordinates in Magnetic Resonance Problems*, Rev. Mod. Phys. **26**, 167 (1954). (cited on page 37)

M. A. Reed, C. Zhou, C. J. Muller, T. P. Burgin, and J. M. Tour, *Conductance of a Molecular Junction*, Science **278**, 252 (1997). (cited on page 2)

J. Reichert, R. Ochs, D. Beckmann, H. B. Weber, M. Mayor, and H. von Löhneysen, *Driving current through single organic molecules*, Phys. Rev. Lett. **88**, 176804 (2002). (cited on page 2)

J. Reichert, H. B. Weber, M. Mayor, and H. von Löhneysen, *Low-temperature conductance measurements on single molecules*, Appl. Phys. Lett. **82**, 4137 (2003). (cited on page 2)

P. Reimann, *Brownian Motors: Noisy Transport far from Equilibrium*, Phys. Rep. **361**, 57 (2002). (cited on pages 4 and 30)

P. Reimann, M. Grifoni, and P. Hänggi, *Quantum Ratchets*, Phys. Rev. Lett. **79**, 10 (1997). (cited on page 30)

M. Rey, M. Strass, S. Kohler, F. Sols, and P. Hänggi, *Transport suppression in heterostructures driven by an ac gate voltage*, Chem. Phys. **319**, 360 (2005). (cited on pages 55 and 57)

H. Sambe, *Steady States and Quasienergies of a Quantum-Mechanical System in an Oscillating Field*, Phys. Rev. A **7**, 2203 (1973).
(cited on pages 27, 28, and 39)

W. Schottky, *Über spontane Stromschwankungen in verschiedenen Elektrizitätsleitern*, Ann. Phys. (Leibzig) **57**, 541 (1918).
(cited on pages 2 and 21)

J. H. Shirley, *Solution of the Schrödinger Equation with a Hamiltonian Periodic in Time*, Phys. Rev. **138**, B979 (1965). (cited on pages 27 and 39)

C. P. Slichter, *Principles of magnetic resonance*, vol. 1 of *Springer Series in Solid-State Sciences* (Springer, Berlin Heidelberg, 1996), 3rd ed.
(cited on page 45)

F. Sols, *Gauge-Invariant Formulation of Electron Linear Transport*, Phys. Rev. Lett. **67**, 2874 (1991). (cited on page 80)

W. Song, A. K. M. Newaz, J. K. Son, and E. E. Mendez, *Drastic reduction of shot noise in semiconductor superlattices*, unpublished; preprint: `arXiv:cond-mat/0510594`. (cited on page 77)

C. A. Stafford and N. S. Wingreen, *Resonant Photon-Assisted Tunneling through a Double Quantum Dot: An Electron Pump from Spatial Rabi Oscillations*, Phys. Rev. Lett. **76**, 1916 (1996).
(cited on pages 4, 60, 62, and 71)

A. D. Stone and A. Szafer, *What is measured when you measure a resistence? – The Landauer formula revisited*, IBM J. Res. Dev. **32**, 384 (1988).
(cited on page 12)

M. Strass, P. Hänggi, and S. Kohler, *Nonadiabatic Electron Pumping: Maximal Current with Minimal Noise*, Phys. Rev. Lett. **95**, 130601 (2005a).
(cited on page 60)

M. Strass, S. Kohler, J. Lehmann, and P. Hänggi, *Transport through a driven three-site system*, Mol. Cryst. Liq. Cryst. **426**, 59 (2005b).
(cited on pages 37, 45, and 82)

M. Switkes, C. M. Marcus, K. Campman, and A. C. Gossard, *An Adiabatic Quantum Electron Pump*, Science **283**, 1905 (1999). (cited on page 59)

P. K. Tien and J. P. Gordon, *Multiphoton Process Observed in the Interaction of Microwave Fields with the Tunneling between Superconductor Films*, Phys. Rev. **129**, 647 (1963). (cited on page 45)

R. Tsu and L. Esaki, *Tunneling in a finite superlattice*, Appl. Phys. Lett. **22**, 562 (1973). (cited on page 54)

J. R. Tucker, *Quantum Limited Detection in Tunnel Junction Mixers*, IEEE J. Quantum Electron. **QE-15**, 1234 (1979). (cited on page 46)

J. R. Tucker and M. J. Feldman, *Quantum detection at millimeter wavelength*, Rev. Mod. Phys. **57**, 1055 (1985). (cited on page 46)

A. Ulman, *An Introduction to Ultrathin Organic Films from Langmuir-Blodgett to Self-Assembly* (Academic Press, Boston, 1991). (cited on page 1)

W. G. van der Wiel, S. De Franceschi, J. M. Elzerman, T. Fujisawa, S. Tarucha, and L. P. Kouwenhoven, *Electron transport through double quantum dots*, Rev. Mod. Phys. **75**, 1 (2003). (cited on page 59)

W. G. van der Wiel, T. Fujisawa, T. H. Oosterkamp, and L. P. Kouwenhoven, *Microwave spectroscopy of a double quantum dot in the low- and high-power regime*, Physica B **272**, 31 (1999). (cited on page 60)

A. Wacker and A.-P. Jauho, *Quantum Transport: The Link between Standard Approaches in Superlattices*, Phys. Rev. Lett. **80**, 369 (1998). (cited on page 80)

M. Wagner, *Photon-assisted transmission through an oscillating quantum well: A transfer-matrix approach to coherent destruction of tunneling*, Phys. Rev. A **51**, 798 (1995). (cited on pages 37, 45, and 55)

M. Wagner and F. Sols, *Subsea Electron Transport: Pumping Deep within the Fermi Sea*, Phys. Rev. Lett. **83**, 4377 (1999). (cited on page 3)

H. B. Weber AND J. Würfel, private communication. (cited on pages 3 and 8)

N. S. WINGREEN, A.-P. JAUHO, AND Y. Meir, *Time-dependent transport through a mesoscopic structure*, Phys. Rev. B **48**, 8487 (1993). (cited on page 80)

Y. XUE AND M. A. Ratner, *Microscopic study of electrical transport through individual molecules with metallic contacts. I. Band lineup, voltage drop, and high-field transport*, Phys. Rev. B **68**, 115406 (2003a). (cited on page 11)

Y. XUE AND M. A. Ratner, *Microscopic study of electrical transport through individual molecules with metallic contacts. II. Effect of the interface structure*, Phys. Rev. B **68**, 115407 (2003b). (cited on page 8)

S. N. Yaliraki, M. KEMP, AND M. A. Ratner, *Conductance of molecular wires: Influence of molecule-electrode binding*, J. Am. Chem. Soc. **121**, 3428 (1999). (cited on page 11)

S. N. Yaliraki AND M. A. Ratner, *Molecule-interface coupling effects on electronic transport in molecular wires*, J. Chem. Phys. **109**, 5036 (1998). (cited on page 8)

N. B. Zhitenev, H. MENG, AND Z. BAO, *Conductance of Small Molecular Junctions*, Phys. Rev. Lett. **88**, 226801 (2002). (cited on page 3)

Acknowledgement

First of all, I would like to thank *Prof. Peter Hänggi* for giving me the chance to work on such a cutting-edge subject like molecular electronics. I enjoyed the stimulating atmosphere in his group and I profited even more from his incredibly broad knowledge. His lively and dedicated manner of practicing physics is truly inspiring.

I owe great thanks to *Sigmund Kohler* for supervising this thesis. He is a very competent teacher and I was fortunate to benefit from working and discussing with him. In particular, I would like to point out the very frank and uncomplicated manner of our collaboration.

I would like to express my gratitude to *Prof. Ulrich Eckern* for acting as a second referee on this thesis. For the careful proof reading and the helpful comments on this script, I am indebted to *Franz Kaiser* and *Martijn Wubs*.

For providing part of his numerical code, I am very thankful to *Sébastien Camalet*. Also *Prof. Gert Ingold*, *Jörg Lehmann* and *Franz Kaiser* with whom I collaborated on different aspects of quantum transport should be mentioned here.

Thanks to the numerous former and present members of the *Theorie I* group for all the lively discussions about physics and non-physics topics. Especially, the *Caffè-Runde* has to be emphasized in that context. A big thank you to *Ralf Uterman* and *Michael Schindler* for providing and taking care of the excellent computer infrastructure.

Financial support by the Graduiertenkolleg 283 *"Nichtlineare Probleme in Analysis, Geometrie und Physik* is gratefully acknowledged. The fruitful collaboration with *Miguel Rey* and *Fernando Sols* in Madrid via the Acción Integrada (no. HA2003-0091) is deeply appreciated, as well.

Finally, I am especially grateful to all the people who cared about me and my work and supported me by their prayers. Most important, I thank my wife *Tanja* for her enduring love and care—without her I would not have made it.